Nonlinear Distortion Analysis of Directly Modulated DFB Lasers under Optical Injection Locking

연세대학교 대학원

전기전자 공학과

서 준 혁

Nonlinear Distortion Analysis of Directly Modulated DFB Lasers under Optical Injection Locking

지도 최 우 영 교수

이 논문을 석사 학위논문으로 제출함

2001 년 12 월 일

연세대학교 대학원

전기·전자공학과

서 준 혁

서준혁의 석사 학위논문을 인준함

심사위원_____인

심사위원_____인

심사위원_____인

연세대학교 대학원

2001 년 12 월 일

Nonlinear Distortion Analysis of Directly Modulated DFB Lasers under Optical Injection Locking

By

Jun-Hyuk Seo

Submitted to the Department of Electrical and Electronic Engineering
in partial fulfillment of the requirements for the Degree
Master of Science

at the

Department of Electrical and Electronic Engineering
The Graduate School
YONSEI University
Seoul, KOREA

December 2001

Index

Figure Index

Table Index

Abstract

Nonlinear Distortion Analysis of Directly Modulated DFB Lasers under Optical Injection Locking

by

Jun-Hyuk Seo

at the

Department of Electrical and Electronic Engineering

The Graduate School

Yonsei University

The nonlinear distortion problems in directly modulated DFB lasers and optical injection locking characteristics for reducing the distortion power are described. Then, as a solution of the injection locking weakness, a new nonlinearity suppression method is suggested. By means of Volterra series expansion of the laser rate equation model, the laser second order and third order intermodulation distortion are calculated analytically. For investigating the optical injection locking characteristics, the laser rate equation model is simulated numerically, and the laser parameter dependent stable locking range is calculated. The optical injection wavelength and power dependence for distortion suppression are also investigated by the injection locked laser frequency response simulation and by experimental observation of second order intermodulation distortion suppression. Finally, for improving the

injection locking technique, sidemode optical injection locking is proposed. The injection locking technique has a weakness for stability, which is related to the stable locking range. By injecting external light into a DFB laser sidemode, the laser distortion is suppressed significantly, and a wider stable locking range is achieved compared to the previously reported main-mode optical injection locking.

Keywords: nonlinear distortion, direct laser modulation, optical injection locking, sidemode optical injection locking, analog fiber optic link, stable locking range, Volterra series, rate equation

I. Introduction

In the past, telecommunication networks were generally classified into three main categories: the public switched telephone network (PSTN), the local-area computer network, and the emerging community antenna television (CATV) network [1]. Such networks mainly provided voice communication services, multimedia oriented services, and broadcast entertainment video signals. However, with increasing computer power and Internet related services, they are merging into one broadband network services. The companies want to serve voice, multimedia, and entertainment altogether. Moreover, new high technology telecommunication networks such as PCS, IMT-2000, and HDTV services are developed and these will prevail soon. To serve these to customers cheap and efficiently, high-speed transmission networks are needed, and optical communication networks are proper for them. Optical networks are usually used as a backbone network, and have several hundreds Gbps data transmission capacity. To apply such high speed to the broadband network services, analog fiber-optic transmission systems are suggested as simple and low cost systems [2].

In the analog fiber-optic transmission systems, multiple analog data signals are transmitted by one or many optical carriers. Because the optical carrier has very large bandwidth and analog data capacity is from several Mbps to tens of Mbps, analog fiber-optic transmission systems can serve tens of channels at a time. Therefore, simple and low cost broadband network services are possible. The analog fiber-optic transmission systems have two kinds of data modulation methods: direct modulation and external modulation. When

considering cost aspect, the direct modulation is preferred. The direct modulation is that the information signals are supplied to the semiconductor lasers directly, and the laser output is data modulated light. With direct modulation method, the semiconductor lasers can transmit information signals multiplexed by RF-range (> 1 GHz) subcarriers. However, when semiconductor lasers are modulated with RF-range electrical signals, nonlinear distortions occur. Such distortions can cause severe system performance degradation, because they cause inter-channel interference that limits the number of channels as well as transmission distance [3, 4].

In low frequency (<1 GHz) applications, the distortion is mainly due to the nonlinear light-versus-current characteristics. However, for direct modulation with RF-range frequency, the nonlinearity introduced by the coupling between photons and electrons in the laser cavity is dominant. This nonlinear coupling also results in the relaxation oscillation resonance [5].

To reduce nonlinear distortions in semiconductor lasers, several methods have been proposed, such as electro-optical feedback and feed-forward compensation [6, 7]. Moreover, Meng *et al*. have reported that laser distortion can be significantly suppressed by injection locking. Light from an external master laser (ML) is used to lock the signal transmitting slave laser (SL) [5]. This technique can increase the laser relaxation oscillation frequency and reduce frequency chirp, which can cause the intrinsic nonlinear distortion suppression in directly modulated semiconductor lasers.

However, the injection locking occurs within the relatively narrow frequency detuning range between the ML and SL. This may limit the applicability of the injection locking technique for practical applications. As a

solution for increasing the detuning range, sidemode injection locking technique is proposed. In this scheme, light is injected into a highly suppressed DFB (Distributed Feedback) laser Fabry-Perot mode instead of the DFB laser main-mode. In sidemode optical injection locking, as the sidemode lasing power is very low, the unstable locking characteristics due to mode beating between the ML and SL do not easily occur, and the stable locking range can be extended.

In this thesis, the distortion characteristics and locking characteristics of injection locked DFB lasers are analyzed and the effects of the sidemode injection locking characteristics in locking range and distortion suppression are investigated. First, Section II deals with nonlinear distortion characteristics of directly modulated DFB lasers with Volterra series expansion and numerical analysis of the laser rate equation model. In Section III, the parameter dependent injection locking bandwidth and the laser nonlinear distortion suppression according to the injection power and wavelengths are investigated. Finally, Section IV deals with the sidemode injection locking characteristics and demonstrate that, by using sidemode injection locking, the nonlinear distortions are suppressed greatly and the stable locking range is extended by a factor of two compared to the main-mode injection locking experimentally.

II. Nonlinear Distortion Characteristics in Laser Diodes

A. Nonlinear Distortions in Laser Diodes

S. M. Salgado, *et al.* said that in subcarrier multiplexed (SCM) optical systems, where broadband signals from different channels are transmitted by a number of high-frequency carriers, the nonlinear response of the semiconductor DFB laser is an important factor in determining system performance and the signal-to-noise ratio [8]. This nonlinear response can cause harmonics and intermodulation distortion products, which are combination of the original frequencies. If the laser is modulated at frequencies f_1, f_2 ($f_2 > f_1$), the light signal in addition to modulations at f_1 and f_2 has components at harmonic frequencies ($2f_1$, $2f_2$, $3f_1$, $3f_2$, …) and at intermodulation frequencies (f_2-f_1, f_2+f_1, $2f_2$-f_1, $2f_1$-f_2, $2f_1$+f_2, $2f_2$+f_1, …), i.e., more generally at frequencies $f_k = mf_1 + nf_2$ (m, n $\in$ integer, $f_k > 0$). The mechanisms of distortion in DFB lasers are considered being related to a combination of relaxation oscillation resonance, light-versus-carrier characteristics (L-I) and nonuniform distributions of the optical field and of the carrier density [3, 4]. In low frequency applications, such as cable TV systems (< 1 GHz), the distortion is mainly due to the nonlinear light-versus-current characteristic (L-I), and dynamic longitudinal variation of the optical field and the carrier density (spatial hole burning) [4]. In contrast, for high-frequency (>1 GHz) SCM systems, such as cellular mobile communication and satellite communication systems, the nonlinearity introduced by the coupling between photons and electrons in the laser cavity becomes dominant

[8, 9, 10]. This phenomenon occurs well near the relaxation resonance frequency.

Fig. 2-1 and 2-2 show the laser nonlinear distortion products in RF spectrum domain. Fig. 2-1 is the one-tone (2.9 GHz) simulation result and Fig 2-2 is two-tone (2.9 GHz and 3 GHz) case. These are the results by numerically solving the following rate equations.

$$\frac{dS}{dt} = [\Gamma g_0 (N - N_t)/(1 + \varepsilon S) - \frac{1}{\tau_p}]S - Rsp \qquad 2-1(a)$$

$$\frac{d\Phi}{dt} = \frac{1}{2}\alpha[\Gamma g_0 (N - N_t)/(1 + \varepsilon S) - \frac{1}{\tau_p}] \qquad 2\text{-}1(b)$$

$$\frac{dN}{dt} = \frac{I}{qV} - \frac{N}{\tau_N} - g_0 (N - N_t)S/(1 + \varepsilon S) \qquad 2\text{-}1(c)$$

These rate equations are derived from a traveling wave description of the field inside the laser cavity. In the above equation, S indicates the photon density of the laser. N and Φ are the carrier density and the phase of photon respectively. Γ is the laser confinement factor, which is field distribution ratio inside the laser active region. g_0 is the differential gain, and N_t is the transparent carrier density. τ_P and τ_N indicate the photon lifetime and carrier lifetime respectively. Lastly ε is gain suppression factor. The values of the parameters are referred from the reference [11] and table I lists the values. The modulation index m (= $I_{modulation}/(I_{bias} - I_{th})$) is 0.2. Fig 2-1(a) shows the harmonic distortion products in optical domain, and fig 2-1(b) reveals the multi-order intermodulation distortion products (IMPs) as well as harmonic distortion products. These two figures show well the distortion phenomena in directly modulated laser diodes (LDs).

Table I. Laser Parameter and Their Numerical Values [11]

Symbol	Parameter	Value
τ_p	Photon lifetime	2 ps
τ_s	Carrier lifetime	1 ns
g_0	Differential gain	$2.13*10^{-6}$ cm^3/s
α	Linewidth enhancement factor	5
Γ	Confinement factor	0.4
ε	Gain suppression factor	$1.0*10^{-17}$
I_{th}	Threshold current	33.5 mA
N_t	Transparent carrier density	$1.0*10^{18}$ cm^{-3}
β	Spontaneous emission factor	$3*10^{-5}$

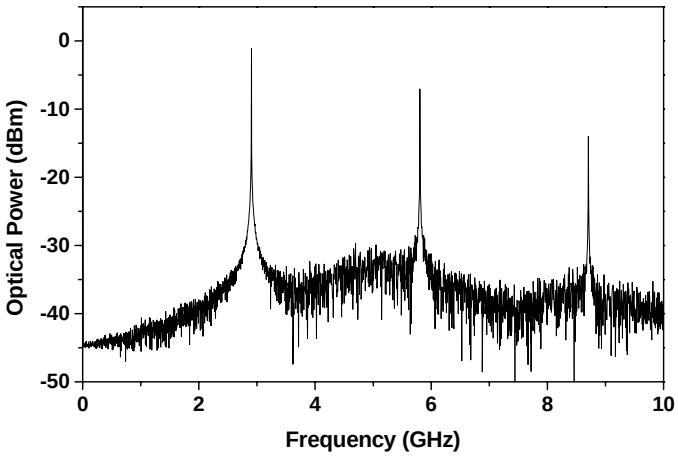

(a)

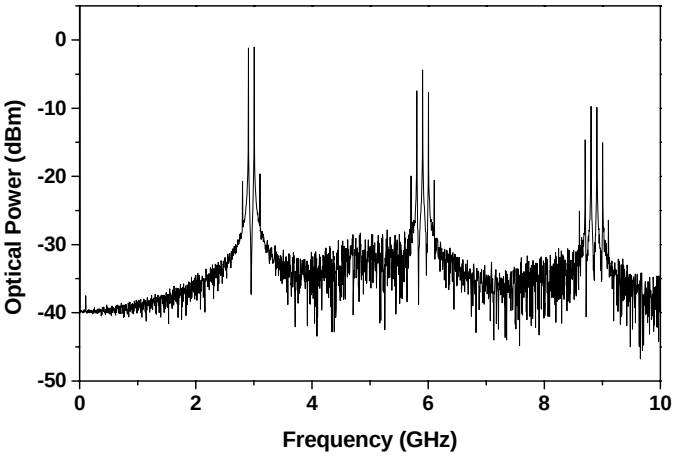

(b)

Figure 2.1 Distortion products power of directly modulated semiconductor lasers. (a) one-tone (2.9 GHz) modulation (b) two-tone (2.9 GHz, 3 GHz) modulation

At the next section, to analyze distortion phenomena more accurately, Volterra functional series expansion of directly modulated LDs will be adapted. Volterra series analysis of laser distortion gives a more tractable and accurate solution because this can include multi-order IMPs for laser nonlinearity as determined by the rate equations and for an arbitrary number of channels.

B. Nonlinear Distortion Modeling in Directly Modulated Laser Diodes by Volterra Series

The basic mathematical theories are almost directly quoted from reference [8].

(1) Volterra Series: frequency domain analysis [8]

In nonlinear systems where the distortion is frequency dependent the nonlinearity can be best represented by a Volterra functional series described as a 'power series with memory' [12, 13]. The semiconductor laser is then viewed as a nonlinear system where the output $p = p_0+p(t)$, the normalized photon density, is some functional input $j = j_0+j(t)$, the normalized current density, where

$$p(t) = \sum_{n=1}^{\infty} p_n(t) \qquad 2\text{-}2$$

$$p_n(t) = \int_{-\infty}^{\infty} \cdots \int_{-\infty}^{\infty} h_n(\tau_1,\ldots,\tau_n) \prod_{r=1}^{n} j(t-\tau_r) d\tau_r \qquad 2\text{-}3$$

p_0 and j_0 are the corresponding steady-state values and $h_n(t_1,\ldots,t_n)$ is the laser nonlinear impulse response of order n. The Fourier transform of $h_n(t_1,\ldots,t_n)$

$$H_n(f_1,\ldots,f_n) = \int_{-\infty}^{\infty} \cdots \int_{-\infty}^{\infty} h_n(\tau_1,\ldots,\tau_n) \prod_{r=1}^{n} e^{-i2\pi f_r t} d\tau_r \qquad 2\text{-}4$$

is the laser nonlinear transfer function of order n. Thus, the use of Volterra series is a generalization of linear system theory. The photon density can also be written as a function of the input spectrum J(f)

$$P_n(t) = \int_{-\infty}^{\infty} \ldots \int_{-\infty}^{\infty} h_n(\tau_1,\ldots,\tau_n) \prod_{r=1}^{n} J(f_r) e^{i2\pi f_r t} d f_r \qquad 2\text{-}5$$

from which the output spectrum is obtained by Fourier transform.

$$P(f) = \sum_{n=1}^{\infty} P_n(f) \qquad 2\text{-}6$$

$$P_n(f) = \int_{-\infty}^{\infty} \ldots \int_{-\infty}^{\infty} H_n(\tau_1,\ldots,\tau_n) \delta(f - f_1 - \ldots - f_n) \prod_{r=1}^{n} J(f_r) d f_r \qquad 2\text{-}7$$

The representation of the output by its Volterra expansion, eqn. 2-5, requires the nonlinear transfer functions $H_n(f_1,\ldots,f_n)$.

(2) Determination of nonlinear transfer functions [8, 12, 13]

The method described in reference 12, 13 to evaluate the transfer function is called the 'probing' or 'harmonic input' method because it assumes the input to be given by a sum of exponentials

$$j(t) = e^{i2\pi f_1 t} + e^{i2\pi f_2 t} + \ldots + e^{i2\pi f_n t} \qquad 2\text{-}8$$

where f_r, r=1, 2, …, n are linearly independent. Thus, when the input is eqn. 2-8, H_n is given by $H_n(f_1,\ldots,f_n)$ = {coefficient of the n!exp[j($2\pi f_1$+…+$2\pi f_2$)t] term in the expansion of $p_n(t)$}. It enables to compute $H_1(f_1)$, $H_1(f_2)$, $H_2(f_1, f_2)$, … in succession. Thus, when we replace j(t) by exp(j$2\pi f_1$)t in the system equations and assume

$$p_n(t) = \sum_{n=1}^{\infty} n! c_k e^{i2\pi f_1 t} \qquad 2\text{-}9$$

$H_1(f_1)$ is equal to c_1. Similarly, $H_2(f_1, f_2)$ is equal to c_{11} where

$$j(t) = e^{i2\pi f_1 t} + e^{i2\pi f_2 t} \qquad 2\text{-}10$$

$$P_n(t) = \sum_{k=0}^{\infty}\sum_{l=0}^{\infty} n! c_{kl} e^{[i2\pi(kf_1+lf_2)t]} \qquad 2\text{-}11$$

$c_{00} = 0$, $c_{10} = H_1(f_1)$, $c_{01} = H_1(f_2)$

and $H_3(f_1, f_2, f_3)$ is equal to c_{111} in an analogous triple sum where

$c_{000} = 0$, $c_{110} = H_2(f_1, f_2)$, $c_{100} = H_1(f_1)$, $c_{010} = H_1(f_2)$, ⋯ .

Generally, when the input j(t) is eqn. 2-8, the resulting output signal is then

$$p_n(t) = \sum_{f} \frac{n!}{m_1!\cdots m_n!} H_n(m_1[f_1],\ldots,m_n[f_n]) \prod_{r=1}^{n} e^{i2\pi m_r f_r t} \qquad 2\text{-}12$$

where

$$\sum_{r=1}^{n} m_r = n \quad \text{and} \quad m_r[f_r] = m_r \text{ times } (f_r, \ldots, f_r)$$

that is m_r consecutive arguments in $H_n(\ )$ having the same frequency f_r: f under the summation indicates that the sum includes all the frequencies generated by the nth-order nonlinear transfer function $f = m_1f_1 + m_2f_2 + \ldots + m_nf_n$ associated with the distinct sets $\{m_1, \ldots, m_n\}$. In this equation there is a term of order n corresponding to $m_1 = \ldots = m_n = 1$ given by

$$n! H_n(f_1,\ldots,f_n) e^{i2\pi(f_1+\ldots+f_n)t} \qquad 2\text{-}13$$

and there are no more terms associated with $\exp[i2\pi(f_1+\ldots+f_n)t]$ than this term because $f_1,\ldots, f_n$ were assumed to be linearly independent. Therefore, the nth nonlinear transfer function $H_n(f_1, \ldots, f_n)$ can be determined as the coefficient of $n!\ H_n \exp[i2\pi(f_1+\ldots+f_n)t]$ in the laser output when the input current is the sum of exponentials (eqn. 2-8). This suggests the use of the perturbation technique to determine all the transfer functions from the single-mode rate equation, 2-1.

(3) Laser nonlinear transfer functions

To determine the transfer functions of the photon, the rate equations in eqns. 2-1 are used. In eqn. 2-1, the rate equation about the photon phase, 2-1(b), will not be used here because the distortions affected by lasing frequency modulation (chirping) are out of concern. The photon transfer function is set at H(f) and carrier transfer function is set at G(f). In case of distortions, only photon transfer functions are related, but the carrier transfer functions are needed to get high-order photon transfer functions.

First, $H_1(f_1)$ and $G_1(f_1)$ are determined by following procedures. The photon density and carrier density is set at $P = P_0 + P(t)$, and $N = N_0 + N(t)$ where

$$P(t) = H_1(f_1)e^{i2\pi f_1 t},\ N(t) = G_1(f_1)e^{i2\pi f_1 t} \qquad 2\text{-}14$$

and P_0 and N_0 is steady state value of photon and carrier respectively. Then, I is set $\exp(i2\pi f_1 t)$ and by inserting these values in the rate equations, the nonlinear transfer functions are determined like that:

$$H_1(f_1) = \frac{\Gamma[\tau_n g_0(1-\varepsilon P_0)P_0 + \beta]\tau_n}{qV\phi_{f1}} \qquad 2\text{-}15$$

$$G_1(f_1) = \frac{\tau_n \chi_{f1}}{qV\phi_{f1}} \qquad 2\text{-}16$$

where

$$\varphi_{f1} = i2\pi\tau_n f_1 + \tau_n g_0(1-\varepsilon P_0)P_0 + 1 \qquad 2\text{-}17$$

$$\chi_{f1} = i2\pi\tau_n f_1 - \tau_n \Gamma g_0(N_0 - N_t)(1-2\varepsilon P_0) + \tau_n/\tau_p \qquad 2\text{-}18$$

$$\phi_{f1} = \varphi_{f1}\chi_{f1} + \Gamma[\tau_n g_0(1-\varepsilon P_0)P_0 + \beta][\tau_n g_0(N_0 - N_t)(1-2\varepsilon P_0)] \qquad 2\text{-}19$$

Next, the second order transfer function, $H_2(f_1, f_2)$ and $G_2(f_1, f_2)$ can be calculated using eqn. 2-15 and 2-16. As explained before, input and output are set again like that.

$$P = P_0 + P(t), \quad P(t) = H_1(f_1)e^{i2\pi f_1 t} + H_1(f_2)e^{i2\pi f_2 t} + 2!H_2(f_1, f_2)e^{i2\pi(f_1+f_2)t} \tag{2-20}$$

$$N = N_0 + N(t), \quad N(t) = G_1(f_1)e^{i2\pi f_1 t} + G_1(f_2)e^{i2\pi f_2 t} + 2!G_2(f_1, f_2)e^{i2\pi(f_1+f_2)t} \tag{2-21}$$

$$I = e^{i2\pi f_1 t} + e^{i2\pi f_2 t} \tag{2-22}$$

When these input and output are inserted into the rate equations, the second order transfer functions can be determined.

$$H_2(f_1, f_2) = \frac{\frac{\tau_n}{\tau_p}\varphi_{f1f2}C_1 - \Gamma[\tau_n g_0(1-\varepsilon P_0)P_0 + \beta]D_1}{\phi_{f1f2}} \tag{2-23}$$

$$G_2(f_1, f_2) = \frac{-\tau_n^2 g_0(N_0 - N_t)(1-2\varepsilon P_0)C_1 - D_1\chi_{f1f2}}{\tau_p\phi_{f1f2}} \tag{2-24}$$

where

$$\varphi_{f1f2} = i2\pi\tau_n(f_1 + f_2) + \tau_n g_0(1-\varepsilon P_0)P_0 + 1 \tag{2-25}$$

$$\chi_{f1f2} = i2\pi\tau_n(f_1 + f_2) - \tau_n\Gamma g_0(N_0 - N_t)(1-2\varepsilon P_0) + \tau_n/\tau_p \tag{2-26}$$

$$\phi_{f1f2} = \varphi_{f1f2}\chi_{f1f2} + \Gamma[\tau_n g_0(1-\varepsilon P_0)P_0 + \beta] \times[\tau_n g_0(N_0 - N_t)(1-2\varepsilon P_0)] \tag{2-27}$$

$$C_1 = \frac{1}{2}\tau_p\Gamma g_0[(1-2\varepsilon P_0)(G_1(f_1)H_1(f_2) + G_1(f_2)H_1(f_1)) - 2(N_0 - N_t)\varepsilon H_1(f_1)H_1(f_2)] \tag{2-28}$$

$$D_1 = \frac{1}{2}\tau_n g_0[(1-2\varepsilon P_0)(G_1(f_1)H_1(f_2)+G_1(f_2)H_1(f_1)) - 2(N_0-N_t)\varepsilon H_1(f_1)H_2(f_2)] \quad \text{2-29}$$

Finally, the third order transfer function of photon is determined by means of first order and second order transfer functions. The procedures are also the same as before, and the input and output are released like that.

$$P = P_0 + P(t),\quad P(t) = H_1(f_1)e^{i2\pi f_1 t} + H_1(f_2)e^{i2\pi f_2 t} + H_1(f_3)e^{i2\pi f_3 t} + 2!H_2(f_1,f_2)e^{i2\pi(f_1+f_2)t} + 2!H_2(f_2,f_3)e^{i2\pi(f_2+f_3)t} + 2!H_2(f_1,f_3)e^{i2\pi(f_1+f_3)t} + 3!H_3(f_1,f_2,f_3)e^{i2\pi(f_1+f_2+f_3)t} \quad \text{2-30}$$

$$N = N_0 + N(t),\quad N(t) = G_1(f_1)e^{i2\pi f_1 t} + G_1(f_2)e^{i2\pi f_2 t} + G_1(f_3)e^{i2\pi f_3 t} + 2!G_2(f_1,f_2)e^{i2\pi(f_1+f_2)t} + 2!G_2(f_2,f_3)e^{i2\pi(f_2+f_3)t} + 2!G_2(f_1,f_3)e^{i2\pi(f_1+f_3)t} + 3!G_3(f_1,f_2,f_3)e^{i2\pi(f_1+f_2+f_3)t} \quad \text{2-31}$$

$$I = e^{i2\pi f_1 t} + e^{i2\pi f_2 t} + e^{i2\pi f_3 t} \quad \text{2-32}$$

From these input and output, the determined third order photon transfer function is that

$$H_3(f_1,f_2,f_3) = \frac{\frac{\tau_n}{\tau_p}\varphi_{f1f2f3}C_2 - \Gamma[\tau_n g_0(1-\varepsilon P_0)P_0+\beta]D_2}{\phi_{f1f2f3}} \quad \text{2-33}$$

where

$$\varphi_{f1f2f3} = i2\pi\tau_n(f_1+f_2+f_3) + \tau_n g_0(1-\varepsilon P_0)P_0 + 1 \quad \text{2-34}$$

$$\chi_{f1f2f3} = i2\pi\tau_n(f_1+f_2+f_3) - \tau_n\Gamma g_0(N_0-N_t)(1-2\varepsilon P_0) + \tau_n/\tau_p \quad \text{2-35}$$

$$\phi_{f1f2f3} = \varphi_{f1f2f3}\chi_{f1f2f3} + \Gamma[\tau_n g_0(1-\varepsilon P_0)P_0+\beta] \times[\tau_n g_0(N_0-N_t)(1-2\varepsilon P_0)] \quad \text{2-36}$$

$$
\begin{aligned}
C_2 = \frac{1}{3}\tau_p \Gamma g_0 [&(1-2\varepsilon P_0)(H_1(f_1)G_2(f_2,f_3)+H_1(f_2)G_2(f_1,f_3) \\
&+H_1(f_3)G_2(f_1,f_2)+G_1(f_1)H_2(f_2,f_3)+G_1(f_2)H_2(f_1,f_3) \\
&+G_1(f_3)H_2(f_1,f_2))-2\varepsilon(N_0-N_t)(H_1(f_1)H_2(f_2,f_3) \\
&+H_1(f_2)H_2(f_1,f_3)+H_1(f_3)H_2(f_1,f_2)) \\
&-\varepsilon(G_1(f_1)H_1(f_2)H_1(f_3)+G_1(f_2)H_1(f_1)H_1(f_3) \\
&+G_1(f_3)H_1(f_1)H_1(f_2))]
\end{aligned}
\qquad \text{2-37}
$$

$$
\begin{aligned}
D_2 = \frac{1}{3}\tau_n g_0 [&(1-2\varepsilon P_0)(H_1(f_1)G_2(f_2,f_3)+H_1(f_2)G_2(f_1,f_3) \\
&+H_1(f_3)G_2(f_1,f_2)+G_1(f_1)H_2(f_2,f_3)+G_1(f_2)H_2(f_1,f_3) \\
&+G_1(f_3)H_2(f_1,f_2))-2\varepsilon(N_0-N_t)(H_1(f_1)H_2(f_2,f_3) \\
&+H_1(f_2)H_2(f_1,f_3)+H_1(f_3)H_2(f_1,f_2)) \\
&-\varepsilon(G_1(f_1)H_1(f_2)H_1(f_3)+G_1(f_2)H_1(f_1)H_1(f_3) \\
&+G_1(f_3)H_1(f_1)H_1(f_2))]
\end{aligned}
\qquad \text{2-38}
$$

(4) Laser nonlinear response [8, 13]

The laser response to a sum of narrow-band signals will now be derived. Let the input signal current be a sum of K narrow-band signals centered at f_k

$$
\begin{aligned}
j(t) &= \sum_{k=1}^{K} \frac{1}{2}[z_k(t)e^{i2\pi f_k t} + z_k(t)^* e^{-i2\pi f_k t} \\
&= \frac{1}{2}\sum_{k=-K}^{K} z_k(t)e^{-i2\pi f_k t}
\end{aligned}
\qquad \text{2-39}
$$

where $z_k(t)$ is the complex envelope representation of $j_k(t)$, $z_k(t)^*=z_{-k}(t)$ and $z_0(t)=0$. Defining $Z_k(f)$ as the Fourier transform of $z_k(t)$ and denoting $Z_k(-f)^*$ and $-f_k$ by $Z_{-k}(f)$ and f_{-k}, respectively, the spectrum $J_k(f)$ of $j_k(t)$ is

$$
\begin{aligned}
J_k(f) &= \frac{1}{2}\sum_{k=1}^{K}[Z_k(f-f_k)+Z_k(-f-f_k)] \\
&= \frac{1}{2}\sum_{k=-K}^{K} Z_k(f-f_k)
\end{aligned}
\qquad \text{2-40}
$$

The photon density expanded as a Volterra series becomes

$$p(t) = \sum_{n=1}^{\infty}\sum_{k}\left\{\mathrm{Re}\frac{n!2^{-n+1}}{m_{-K}!\cdots m_K!}\left[\int_{-\infty}^{\infty}\cdots\int_{-\infty}^{\infty} H_n(f_1 - f_{k1},..., f_n - f_{kn})\right.\right.$$
$$\left.\left.\times\prod_{r=1}^{n} Z_{kr}(f_r)e^{i2\pi f_r t}df_r\right]\exp\left(i2\pi\sum_{r=1}^{n} f_{kr}t\right)\right] \qquad 2\text{-}41$$
$$= \sum_{n=1}^{\infty}\sum_{k} p_{nf}(t)$$

where the k under the summation indicates that the sum includes all the distinct sets $\{k_1, \ldots, k_n\}$ with k_r=-K, …, K and m_k=0, …n is the number of times each distinct k_r occurs in this set, such that

$$\sum_{k=-K}^{K} m_k = n \qquad 2\text{-}42$$

By comparison of eqn. 2-39 and 2-41, it can be concluded that when the input current consists of a sum of narrow-band signals, the laser generates new narrow-band components centered at all carrier intermodulation frequencies. $P_{nf}(t)$ represents the photon density waveform centered at frequency

$$f = \sum_{r=1}^{n} f_{kr} = \sum_{k=-K}^{K} m_k f_k \qquad 2\text{-}43$$

generated by intermodulation of the input signal components centered at f_{k1}, …, f_{kn} which has complex envelope $q_{nf}(t)$

$$p_{nf}(t) = \mathrm{Re}\left\{q_{nf}(t)\exp\left(i2\pi\sum_{r=1}^{n} f_{kr}t\right)\right\} \qquad 2\text{-}44$$

given by

$$q_{nf}(t) = \frac{n!2^{-n+1}}{m_{-K}!\cdots m_K!}\int_{-\infty}^{\infty}\cdots\int_{-\infty}^{\infty} H_n(f_1 - f_{k1},..., f_n - f_{kn})\times$$
$$\prod_{r=1}^{n} Z_{kr}(f_r)e^{i2\pi f_r t}df_r \qquad 2\text{-}45$$

Hence p_{nf} is the IMP due to the input signals with carriers at frequencies f_{k1}, …,

f_{kn}. The order of the IMP corresponds to the number of carriers generating this product, with the possibility of n being greater than K and signals intermodulating with themselves.

Therefore, when the input carrier is eqn. 2-39, the complex envelope spectra of the carrier is $Z_k(f)=j_k\delta(f)$ and the complex envelope amplitude, $A(f_{k1}, \ldots, f_{kn})$ of the nth-order IMP due to the carriers at $f_{k1}, \ldots, f_{kn}$ may be found from eqn. 2-44 and 2-45

$$A(f_{k1},..., f_{kn}) = \frac{n!\, j_{k1} \cdots j_{kn}}{2^{-n+1} m_{-N}! \cdots m_N!} H_n(f_{k1},.., f_{kn}), k_1,..., k_n = \pm 1,...,\pm N \quad \text{2-46}$$

The amplitude for three input carriers of typical second and third order IMPs are listed in Table II that shows the same results of reference [8].

(6) Results

Fig. 2-2 shows the results of the envelope amplitude analysis. Solid line is the laser transfer function and dotted line and dot-dash line show the second (f_1+f_2) and third ($2f_1-f_2$) order intermodulation products, respectively. These transfer functions were determined in section B-(3) and the parameters used in this analysis are the same as Table I. The frequency difference between two inputs is 0.1 GHz and the OMD (Optical Modulation Depth) is 0.1. The OMD is assumed to be constant as the number of carriers (N) is increased which means the current per carrier must be decreased by 1/N.

$$j = \frac{OMD \cdot P_0}{N \cdot H_1(0)} \quad \text{2-47}$$

The laser transfer function shows that the resonance frequency is about 5 GHz. The second order amplitude shows the characteristics of second order IMPs well. In case of second order IMPs, there are two peak points at resonance

Table II. Amplitude of second and third order IMPs

n	m_{-3}	m_{-2}	m_{-1}	m_1	m_2	m_3	Frequency	Amplitude
2	0	0	0	2	0	0	$2f_1$	$\frac{1}{2} j_1^2 H_2(f_1, f_1)$
2	0	0	0	1	1	0	f_1+f_2	$j_1 j_2 H_2(f_1, f_2)$
3	0	1	0	2	0	0	$2f_1-f_2$	$\frac{3}{4} j_1^2 j_2^* H_3(f_1, f_1, -f_2)$
3	0	0	1	0	2	0	$2f_2-f_1$	$\frac{3}{4} j_1^* j_2^2 H_3(-f_1, f_2, f_2)$
3	1	0	0	1	1	0	$f_1+f_2-f_3$	$\frac{3}{2} j_1 j_2 j_3^* H_3(f_1, f_2, -f_3)$
3	0	1	0	1	0	1	$f_1-f_2+f_3$	$\frac{3}{2} j_2 j_2^* j_3 H_3(f_1, -f_2, f_3)$
3	0	0	1	0	1	1	$-f_1+f_2+f_3$	$\frac{3}{2} j_1^* j_2 j_3 H_3(-f_1, f_2, f_3)$

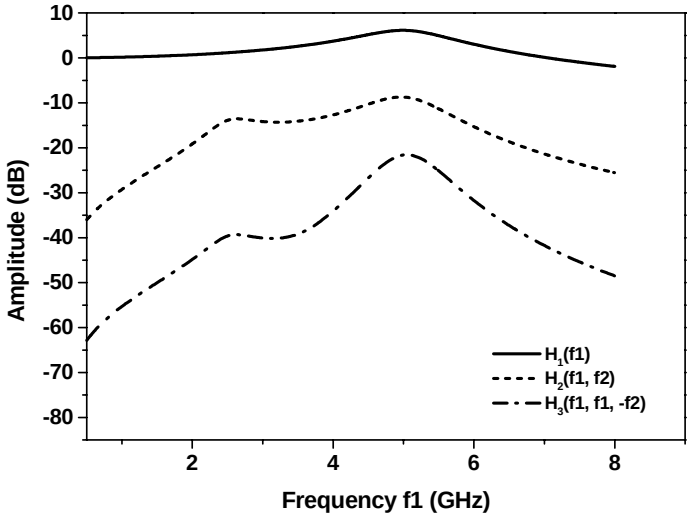

Figure 2.2 Envelope amplitude of laser transfer functions. Solid line: $H_1(f_1)$ f_1 component, Dotted line: $H_2(f_1, f_2)$ f_1+f_2 component, Dot-dash line: $H_3(f_1, f_1, -f_2)$ $2f_1-f_2$ component.

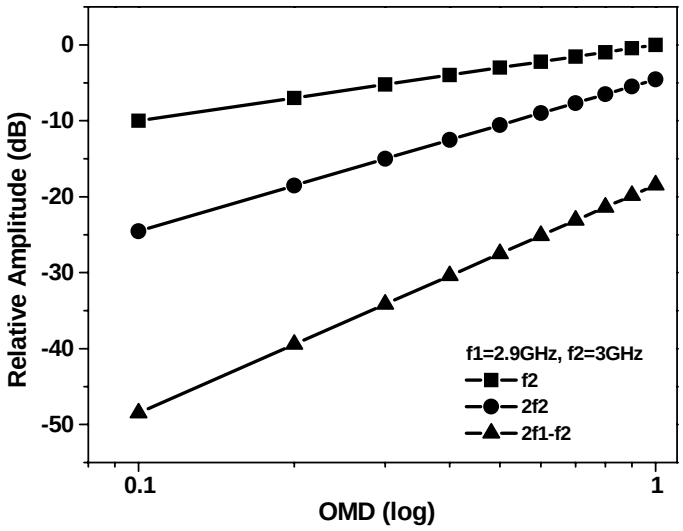

Figure 2.3 Relative amplitude of distortion products according to the log scaled OMD.

frequency and half resonance frequency. When the modulation frequencies are at resonance frequency, the amplitude of all the modulation frequencies are increased and the laser nonlinearity is maximized so that the second order IMPs have the maximum value. In case of half resonance frequency, because the second order IMPs are increased by the laser resonance peak, the second order IMPs can have a large value. The third order IMPs have the maximum at resonance frequency. These results well show the trend that resonance peak is greatly affecting the IMPs.

Fig. 2-3 shows the OMD dependence of modulation products. The results are relative power to the fundamental frequency power at OMD 1. When the scale of x-axis (OMD) is converted to log scale, the slope of the fundamental frequency power is one, and the slope of the second and third order IMP is two and three, respectively. Finally, fig. 2-4 indicates one distortion example of the three-carrier laser modulation. It is the IMPs at f_1-Δf. Δf is 0.1 GHz and f_2 is f_1+Δf and f_2 is f_1+2Δf. In case of three inputs, two third order IMPs (f_1+f_2-f_3, and 2f_1-f_2) contribute to the IMPs at f_1-Δf. Therefore, the envelope amplitude of this case can be calculated like that.

$$A(f_1-\Delta f)=\frac{3}{4}j_1^2 j_2^* H_3(f_1, f_1,-f_2)+\frac{3}{2}j_1 j_2 j_3^* H_3(f_1, f_2,-f_3) \qquad 2\text{-}48$$

The analysis result is similar to the third order IMP at fig. 2-2 because these two third order IMPs have similar trends in frequency dependent amplitude.

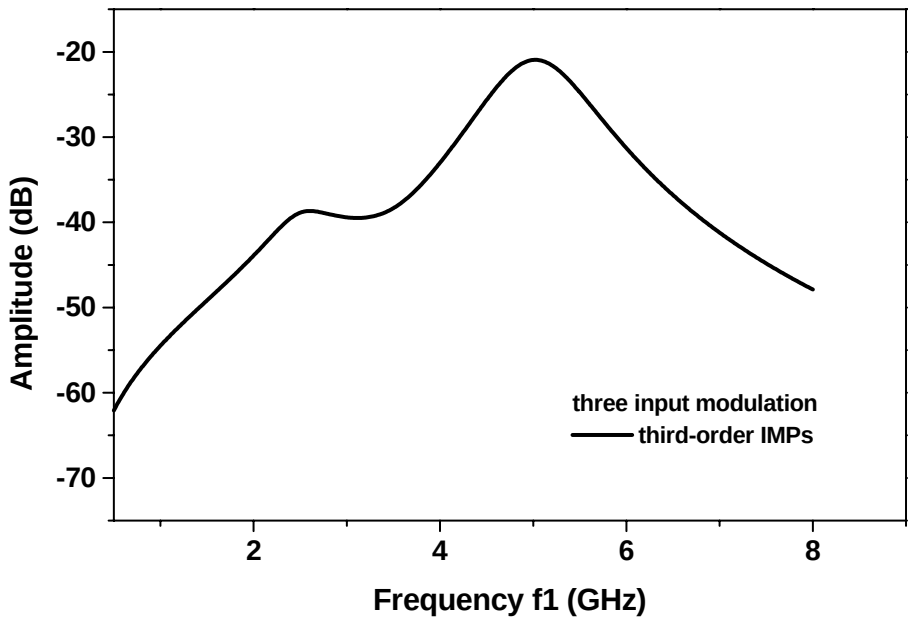

Figure 2.4 Envelope amplitude of third order IMPs according to the three-input modulation. The tree inputs are f_1, $f_2=f_1+\Delta f$, $f_3=f_1+2\Delta f$, $\Delta f=0.1$ GHz and this is the distortion amplitude at $f_1-\Delta f$: $A(f_1-\Delta f) = A(f_1+f_2-f_3) + A(2f_1-f_2)$.

III. Nonlinear Distortion Suppression of Injection Locked DFB Lasers

The direct laser modulation with RF-range frequency has been attracted in analog fiber-optic systems, especially SCM systems because of its low cost and simplicity. However, as shown in section II, when lasers are modulated with RF-range electrical signals, the laser diode (LD) nonlinearities become a key issue in the system performance because it can impose signal distortions. These distortions cause inter-channel interference, which limits the number of channels as well as transmission distance. To cope with this distortion problem, several methods are introduced such as feedforward compensation [7], predistortion [14, 15], and electro-optical feedback methods [6]. In 1997, it has been theoretically shown that the intrinsic dynamic distortion can be substantially suppressed by using optical injection locking to increase the relaxation oscillation frequency [16]. In 1999, X. J. Meng *et. al*. has shown the experimental result of distortion suppression by optical injection locking [5].

The injection locking method is that when an external laser source (Master Laser: ML) light is injected into an operating laser (Slave Laser: SL), the SL is locked to the ML, and the operation of the SL follows the ML. When locking occurs, relaxation oscillation frequency of the SL increases. In RF-range (>1 GHz) laser modulation, the distortion products are greatly influenced by laser relaxation oscillation. Therefore, the relaxation oscillation frequency increase can reduce the laser nonlinear distortion products. Furthermore, the injection locking technique has another merits such as laser narrow linewidth, chirp reduction, and mode partition noise reduction. Therefore, by using injection

locking to suppress nonlinear distortion, the analog system performance can be improved greatly.

A. Injection Locking Characteristic Analysis

To investigate the locking characteristics in the injection locked laser, it is needed a laser model which contains the external light injection effects. The equations below are adequate for this purpose [17]. These rate equations are similar to the eqn. 2-1, but contain E-field characteristics of external light injection.

$$\frac{dS}{dt} = \Gamma g_0 \frac{(N - N_t)}{(1 - \varepsilon S)} S - \frac{S}{\tau_p} + \frac{\beta N}{\tau_n} + 2K_c \sqrt{S \cdot S_{inj}} \cos(\Phi_{inj} - \Phi) \qquad 3\text{-}1(a)$$

$$\frac{d\Phi}{dt} = \frac{1}{2}\alpha \left\{ \frac{(N - N_t)}{(1 - \varepsilon S)} - \frac{1}{\tau_p} \right\} - 2\pi\Delta f + K_c \sqrt{\frac{S_{inj}}{S}} \sin(\Phi_{inj} - \Phi) \qquad 3\text{-}1(b)$$

$$\frac{dN}{dt} = \frac{I}{qV_a} - g_0 (N - N_t) S - \frac{N}{\tau_n} \qquad 3\text{-}1(c)$$

In these equations, Φ_{inj} indicates the injection photon phase, and K_c is the longitudinal mode spacing that is related to the coupling of externally injected wave. Δf is the frequency difference between the ML and SL: the value subtracting the SL frequency from the ML frequency. The other parameters are the same as eqn. 2-1.

Based on these rate equations, small signal analysis is performed at first. By small signal analysis, the stable locking range can be obtained [18]. In case of injection locking, the laser locking is determined by the frequency difference, Δf and the power ratio defined as the ratio of the ML power to the

SL power. To use injection locking technique, these parameters should fulfill the stable locking condition. Therefore, the stable locking condition should be analyzed at first.

For small signal analysis, the parameter S, N, Φ, and I are represented by

$$S(t) = S_0 + \delta S \qquad 3\text{-}2(a)$$

$$N(t) = N_0 + \delta N \qquad 3\text{-}2(b)$$

$$\Phi(t) = \Phi_0 + \delta\Phi \qquad 3\text{-}2(c)$$

$$I(t) = I_0 + \delta I \qquad 3\text{-}2(d)$$

S_0, N_0, Φ_0, and I_0 are steady state solutions. By inserting 3-2(a)-(d) into the eqn. 3-1, a set of linearized equations in the frequency domain is obtained.

$$[M]\cdot\begin{bmatrix}\delta S\\ \delta\Phi\\ \delta N\end{bmatrix} = \begin{bmatrix}0\\ 0\\ \dfrac{-1}{qV_a}\delta I\end{bmatrix} \qquad 3\text{-}3$$

where [M] =

$$\begin{bmatrix} A - BS_0 + K_c\sqrt{\dfrac{S_0}{S_{inj}}}\cos\Phi_0 - iw & 2K_c\sqrt{S_{inj}S_0}\sin\Phi_0 & \dfrac{\Gamma\beta}{\tau_n} + CS_0 \\ -\dfrac{1}{2}[\alpha B + K_c\dfrac{1}{S_0}\sqrt{\dfrac{S_{inj}}{S_0}}\sin\Phi_0] & -K_c\sqrt{\dfrac{S_{inj}}{S_0}}\cos\Phi_0 - iw & \dfrac{1}{2}\alpha C \\ -g_0(N_0 - N_t)(1-\varepsilon S_0) + \dfrac{1}{\Gamma}BS_0 & 0 & -D - iw \end{bmatrix} \qquad 3\text{-}4$$

$$A = \Gamma g_0(N_0 - N_t)(1-\varepsilon S_0) - \frac{1}{\tau_p} \qquad 3\text{-}5$$

$$B = \Gamma g_0\varepsilon(N_0 - N_t) \qquad 3\text{-}6$$

$$C = \Gamma g_0(1-\varepsilon S_0) \qquad 3\text{-}7$$

$$D = -g_0(1-\varepsilon S_0)S_0 - \frac{1}{\tau_n} \qquad 3\text{-}8$$

By using this system matrix, the system can be checked for its stability. The eigenvalues of this matrix indicate the pole location. Therefore, when all the eigenvalues are placed in the left-half plane of complex domain, the system is stable. By using the injection power ratio and frequency detuning as parameters, the stability of locked laser is determined. Fig. 3-1 shows the stable locking region. The detuning frequency means the Δf, and the injection ratio means the injection power ratio. This figure shows well the asymmetric locking range, which is due to the linewidth enhancement factor [18].

Based on this locking map, the effects of external light injection on distortion suppression can be investigated. When the stable locking condition is satisfied, the differential equations 3-1(a)-(c) are solved numerically. To solve these differential equations, MATLAB software is used. Especially, ode45 differential equation solver that is based on modified Runge-Kutta method is used. Fig. 3-2 and 3-3 are the result of simulation in optical domain. Fig. 3-2(a) is the one carrier (2.9 GHz) modulation and no external light injected result, and fig. 3-2(b) is the external light injected result. Modulation index (m) is 0.15 and this is defined like that.

$$m = \frac{I_{peak}}{I_{bias} - I_{th}} \qquad 3\text{-}9$$

Here, I_{peak} is the modulation current peak amplitude, and I_{bias} and I_{th} are the laser bias current amplitude and laser threshold current value, respectively. Δf is set at –21 GHz and injection ratio is –8 dB. These values are acquired from the fig. 3-1. As shown in the figure, the second harmonic power is reduced more than 6.5 dB. Fig. 3.3 shows the third order intermodulation suppression by injection locking. More than 3 dB IMD3 suppression is acquired. Because

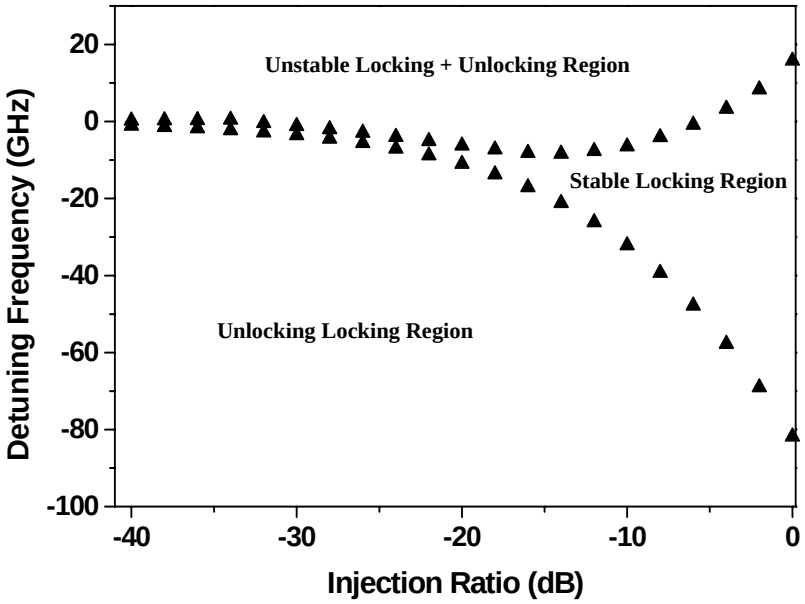

Figure 3.1 Locking region. Injection ratio means the optical injection power ratio: the ratio of the ML power to the SL power, and detuning is the frequency difference between the ML and SL: ML frequency – SL frequency.

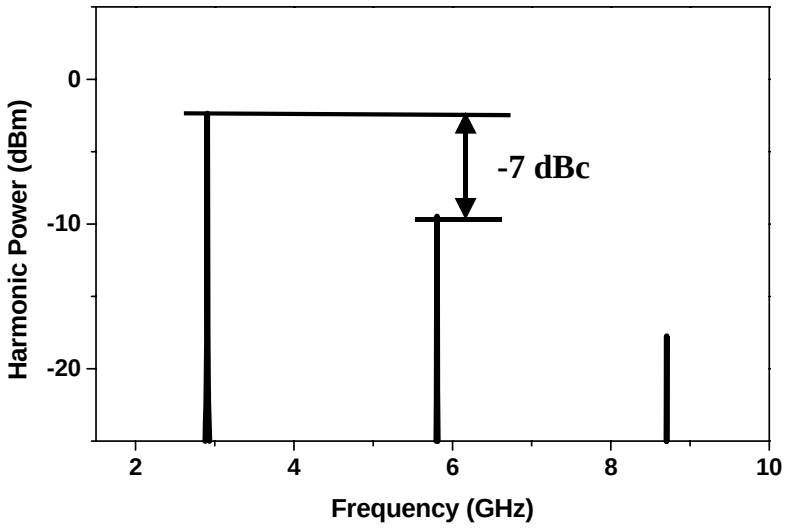

(a)

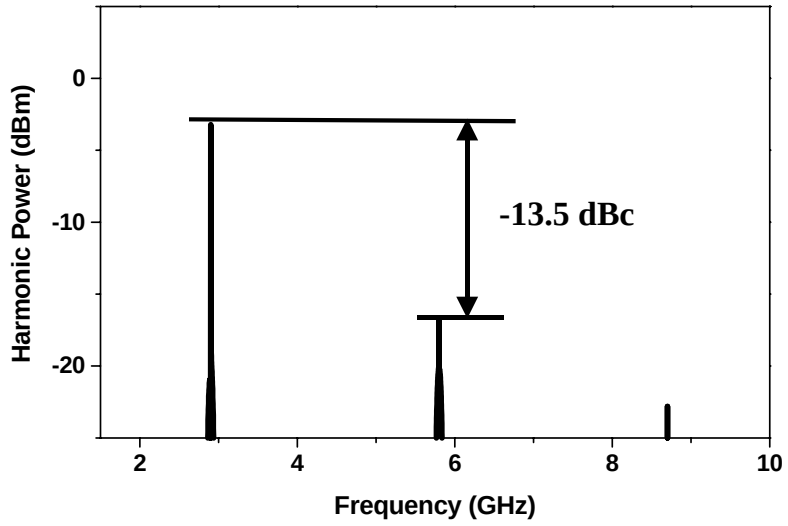

(b)

Figure 3.2 Simulation result of harmonic distortion suppression by optical injection locking. Modulation frequency is 2.9 GHz. (a) the free-running (no optical injection) (b) optical injection locking.

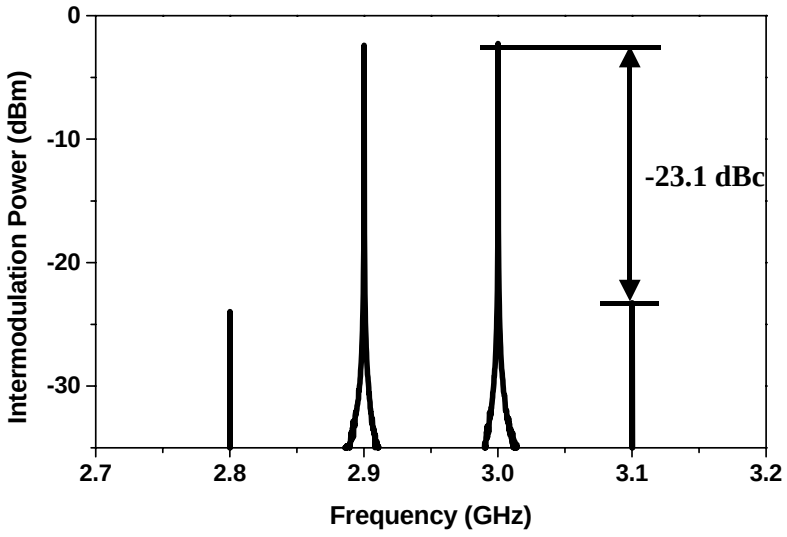

(a)

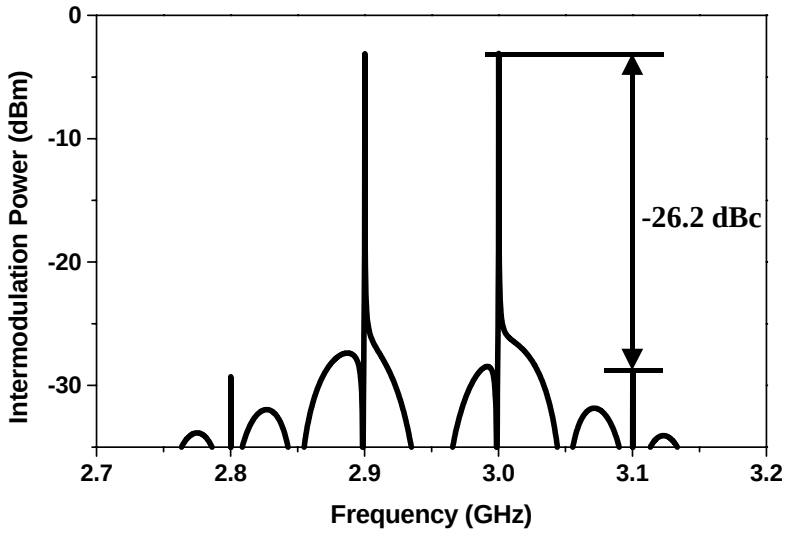

(b)

Figure 3.3 Simulation result of third order intermodulation distortion suppression by optical injection locking. Modulation frequencies are 2.9 GHz and 3.0 GHz. (a) free-running (no optical injection) (b) optical injection locking.

these suppression values are dependent on the external light power and detuning frequency, more distortion suppression can be possible at different condition.

Then, the relaxation oscillation frequency increase phenomenon is simulated. This is a main cause of distortion suppression. From the system matrix, eqn. 3-3, the laser frequency response can be derived. Fig. 3-4 shows the relaxation oscillation frequency increase very well. It is a proof of distortion suppression by injection locking. As the injection light power increases, the relaxation oscillation frequency increases more. Detailed explanations will be given in section III-C.

B. Stable Locking Range according to the Laser Parameters

As explained in section III-A, to reduce the laser nonlinear distortion, the stable locking condition should be satisfied for injection locking application. This stable locking range is greatly influenced by intrinsic laser parameters. Therefore, by comparing these phenomena, laser parameter effects to the locking property can be analyzed. To acquire stable locking range, the simulation method in section III-A is also used.

First, the nonlinear gain suppression factor is considered. This is generally believed the result of spectral hole burning and carrier heating [19, 20]. Fig. 3-5 shows the stable locking range with gain suppression factor and without it. As can be seen in the figure, when the gain suppression factor exists, the stable locking range is greatly increased. This is because the nonlinear gain suppression factor effect is found to cause increased damping of the relaxation

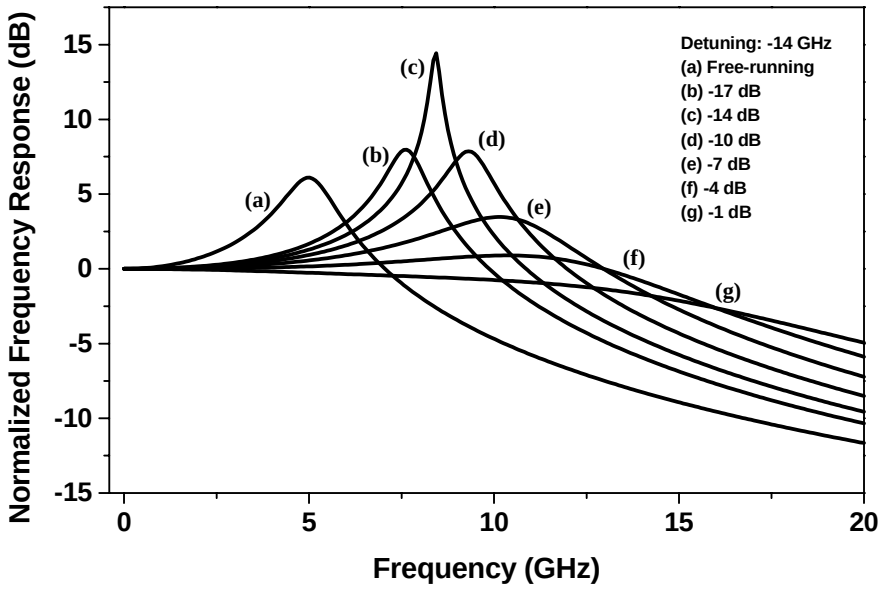

Figure 3.4 Frequency response of injection locked laser. Within the stable locking region, the optical injection power is changed. (a)-(g) are the frequency response at the different injection power ratio.

oscillation [21]. This will result in the suppression of the instability induced by the external perturbation in an optically injected semiconductor laser. Therefore, the effect of nonlinear gain suppression factor on the dynamics of the system is to stabilize the system.

Next, the differential gain effect is analyzed. Fig. 3-6 reveals the stable locking range according to the various differential gain values. By comparing the results, it is observed that when the value of differential gain is reduced, while the other parameters are kept unchanged, the stable locking range is enhanced very much. Clearly, the larger the value of differential gain is, the more unstable the system is. The reason is that a higher differential gain results not only in a higher resonance frequency but also in a reduced damping of the relaxation oscillation [22]. This suggests that a semiconductor laser with a higher differential gain is much easier to be unstable or unlocking.

Fig. 3-7 shows the linewidth enhancement factor dependence in locking range. The linewidth enhancement factor is dependent on laser structures very much, and affects the asymmetric locking characteristics. If α=0, the stable locking range becomes symmetric around the zero frequency detuning. In case of weak injection, which means the injection ratio is less than minus 30 dB, the larger the linewidth enhancement factor is, the narrower the stable locking range is. Moreover, it is said that the unstable characteristics such as chaos and periodic doubling is greatly increased [21]. This is because the linewidth enhancement factor couples the amplitude and phase of the laser field. As can be seen from the rate equation of the laser system, this coupling contributes to the nonlinear dynamics of the lasers very much. However, under strong optical injection, which means the injection ratio is more than -30 dB, the stable

locking range is increased and the locking occurs at very high detuning values. This is a very strange phenomenon, and the reason cannot be explained using the theory of weak injection case.

Finally, the SL bias current effects are considered. Fig. 3-8 is the stable locking range according to the bias current. As shown in the figure, when the bias current is increased, the stable locking range widens at weak injection condition. This phenomenon is explained that when a laser is operated at a higher injection current level, the coherent optical power stored in the cavity is higher, thus allowing the laser to be more resistant to the perturbation of the externally injected optical field [21]. However, in case of strong optical injection, the stable locking range is shrunk at high injection current. This phenomenon is believed that for equalizing the injection power ratio, the external light power should be increased very much and this large external perturbation causes the nonlinear effects.

In this section, the stable locking range is analyzed using intrinsic laser parameters and operation condition such as injection current. The large gain suppression factor affects the stable laser operation, but the large differential gain influences the unstable laser operation in injection locking. In addition, the large linewidth enhancement factor shrinks the stable locking range, and the high injection current widens the stable locking range at weak optical injection. The explanation is mainly referred to the S.K. Hwang's simulation observation and the simulation results are well fitted to his observation [21]. However, the small signal analysis used in this thesis cannot explain entirely the unstable locking phenomena such as chaos, periodic doubling and self-oscillation. Therefore, for more detail analysis of locking phenomena, the

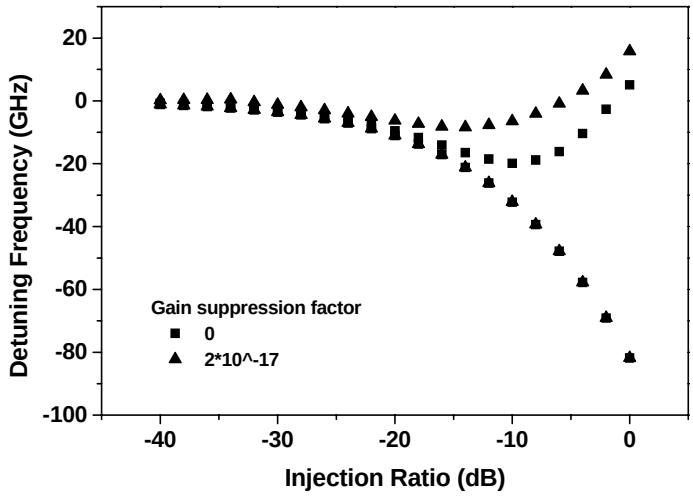

Figure 3.5 Stable locking range according to the gain suppression factor.

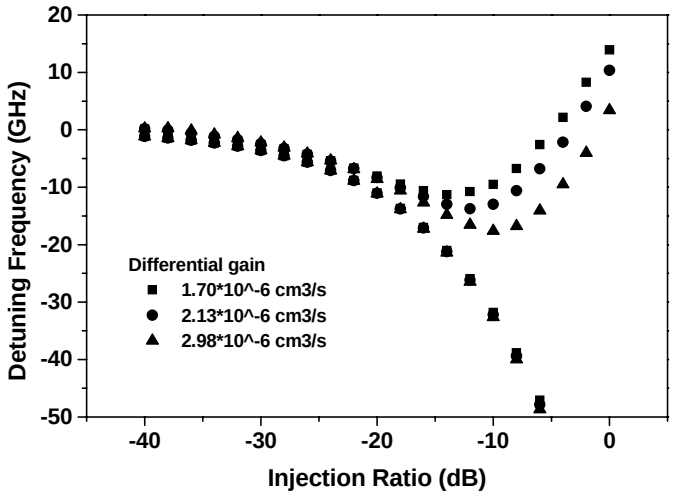

Figure 3.6 Stable locking range according to the differential gain.

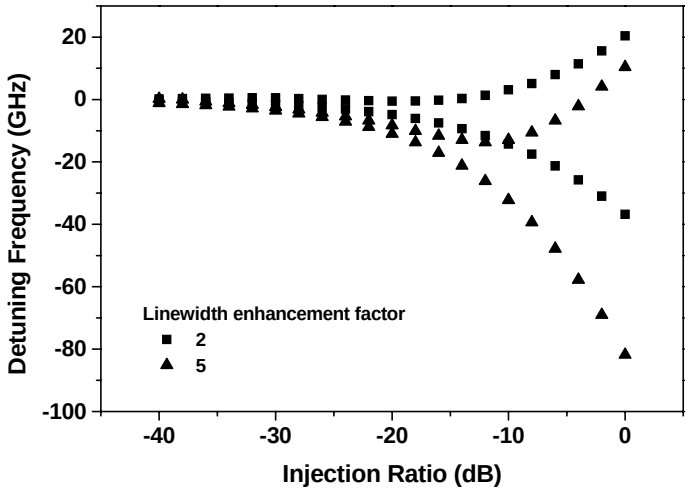

Figure 3.7 Stable locking range according to the linewidth enhancement factor.

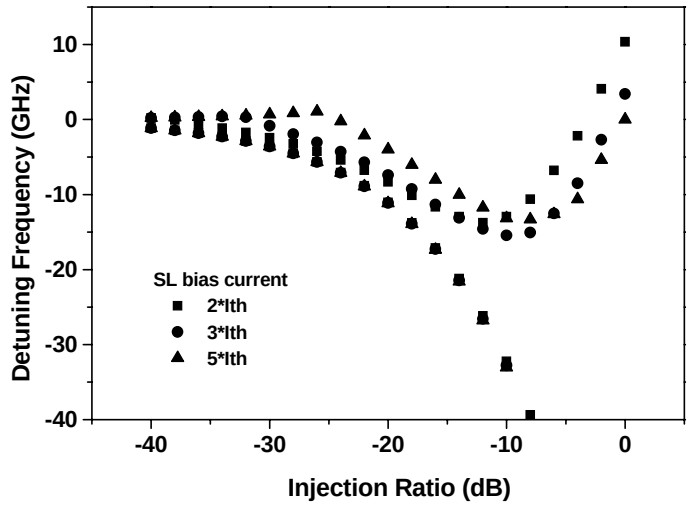

Figure 3.8 Stable locking range according to the SL bias current.

nonlinear phenomena simulation should be executed and the comparison between the simulation and experiment is needed.

C. Injection Wavelength and Power Dependence of Nonlinear Distortion Suppression

From the previous section, III-A, it is investigated numerically and analytically that the nonlinear distortion can be suppressed by means of injection locking. However, the distortion suppression does not equally appear according to the optical injection frequency and power. In this section, optical injection wavelength and power dependence for the nonlinear distortion suppression will be observed.

First, by using the rate equation simulation model, eqn. 3-1, the relaxation oscillation frequency and damping factor change are investigated according to the optical injection wavelength. As can be seen in section III-A, the laser frequency response is calculated by the small signal analysis of the laser rate equations. The injection power ratio is set at –8 dB, and by referring the stable locking range of fig. 3-1, the stable frequency detuning at this injection ratio is determined from –5.5 GHz to –37 GHz. Then, within this range, the frequency response changes are observed. Fig. 3-9(a) and (b) show the results. Fig 3-9(a) is the frequency responses when the detuning frequency is near upper boundary of stable locking region and fig. 3-9(b) is the frequency responses when the detuning frequency is near lower boundary of stable locking region. When the detuning frequency is near upper boundary, the relaxation oscillation frequency increases very much. This indicates that the nonlinear distortion

products caused by the relaxation oscillation can be decreased very much. However, near the upper boundary, nonlinear phenomena such as chaos and frequency doubling can occur very easily. Therefore, when considering the stable system operation, frequency detuning should be apart from the upper boundary. On the other hand, when the detuning frequency is near lower boundary of stable locking region, the relaxation oscillation frequency does not increase greatly. On the contrary, the damping factor increases very much, and the relaxation oscillation is suppressed greatly. In some cases, the damping factor is so large that the modulation bandwidth is decreased. In this condition, the nonlinear distortion products can be suppressed very much. Nevertheless, the modulation signal power is also decreased by damping effects. Therefore, when the decreased signal power is compensated by equalizing to the free-running modulation power, the nonlinear distortion products do not suppressed greatly. However, when reducing the optical injection power, the damping does not occur very severely, and nonlinear distortion suppression can be possible. Generally, when the detuning frequency is near lower boundary, injection locking effects appear very well. Therefore, to maintain other merits of injection locking such as chirp reduction and noise suppression, the optimum optical injection wavelength and power control is needed.

As said briefly before, the optical injection power also affects the laser frequency response, and according to the injection power, the nonlinear distortion suppression effect appears differently. Fig. 3-4 shows the laser frequency response at different optical injection power. The frequency detuning is fixed at –14 GHz. To be sure, the analysis performed within the stable locking range. When the optical injection power increases, the locking

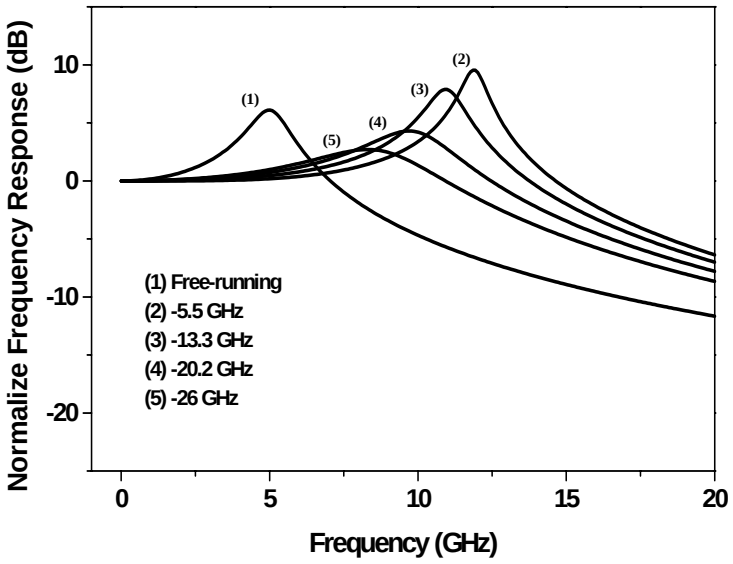

(a)

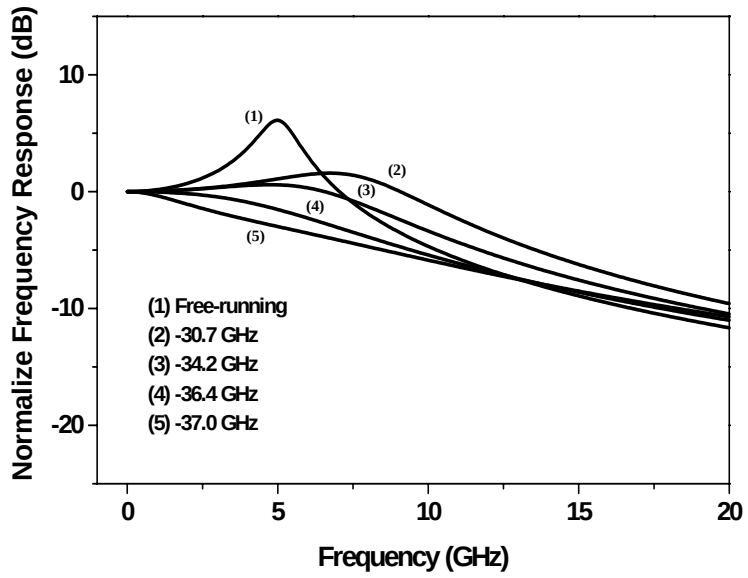

(b)

Figure 3.9 Normalized frequency response of the injection locked SL. (a) Upper boundary of stable locking region cases (b) Lower boundary cases. Injection ratio is fixed at –8 dB.

phenomena occur well. As the injection power increases, the relaxation oscillation frequency increases greatly, and the damping appears very well. However, in the fig. 3-4, first two injection cases do not follow this trend. The reason is that these cases are so close to the upper boundary of stable locking range that the damping effects are weakened.

Next, for verifying these phenomena, IMD2 suppression simulation according to the injection wavelength is also executed. The injection power ratio is also –8 dB and the detuning frequency is selected within the stable locking range. Modulation frequency is 2.8 and 2.9 GHz and the modulation index is 0.1. Fig. 3-10 (a) shows the IMD2 suppression and fig. 3-10 (b) shows the modulation signal power changes according to the injection wavelength. IMD2 suppression is calculated by subtracting the IMD2 at injection locking from the IMD2 at free-running. The modulation signal power degradation values are decided by subtracting the signal power at injection locking from the signal power at free-running. As explained before, the IMD2 suppression near upper stable locking region is due to the relaxation oscillation frequency increase and the IMD2 suppression near lower stable locking region is due to the high damping. The modulation signal power changes are also equal to the expectation. The closer the detuning frequency is near lower stable region boundary, the more the modulation signal power is reduced. Therefore, when the modulation signal power is compensated to the free-running signal power, IMD2 suppression trend is changed. Fig. 3-11 is the compensated result. As the detuning frequency is near the lower stable region boundary, the IMD2 suppression is reduced. The reason is frequency response changes according to the injection wavelength, and the simulation results are well reflected these

effects.

Finally, for verifying the simulation result, the nonlinear distortion suppression is measured experimentally according to the various injection wavelength and power. Fig. 3-12 is the experimental setup. The external cavity tunable light source is used as the ML for simple control of incident wavelength and optical power. For the SL, a commercially available fiber-pigtailed, unisolated DFB laser (Samsung SDL-24) is used. The coupling efficiency from the external light source is about 30% and the threshold current I_{th} is about 7 mA. The lasing wavelength of the SL is stabilized by controlling its temperature and bias current. An optical circulator is used to prevent the unwanted light coupling from the SL to the ML. The locked SL characteristics are observed by optical spectrum analyzer and, after converted into electrical signals, by RF spectrum analyzer.

The SL is modulated with two RF frequencies, 2.8 GHz and 2.9 GHz. Then, within the stable locking range, the distortion suppression is measured according to the different optical injection power and wavelength. The injection wavelength is selected within the stable locking range, and the injection power is fixed at three points, -2 dBm, 2 dBm, and 6 dBm. These values are measured at the output of circulator linked to the SL. For easy measurement, the IMD2 (f_1+f_2) suppression is measured using RF spectrum analyzer. Fig. 3-13 are the experimental results. The modulation signal power is also compensated by equalizing to the free-running fundamental frequency power. These results have very good agreement with the simulation results. Moreover, injection power dependence is also shown in the figure. When the injection light power is high, the IMD2 is increased. The reason is believed

that when the injection power is very high, the damping factor also increases very much and the fundamental signals are greatly suppressed. Therefore, the IMD2 suppression is reduced. However, this phenomenon cannot be proved by IMD2 suppression simulation. At the experimental conditions, the modulation signal power is greatly suppressed when the injection power is high. On the contrary, in the simulation, the modulation signal power does not degrade severely like experiment. The reasons are believed that the simulation models may not explain the injection power dependence exactly or more critical causes for reduced modulation signal power may exist.

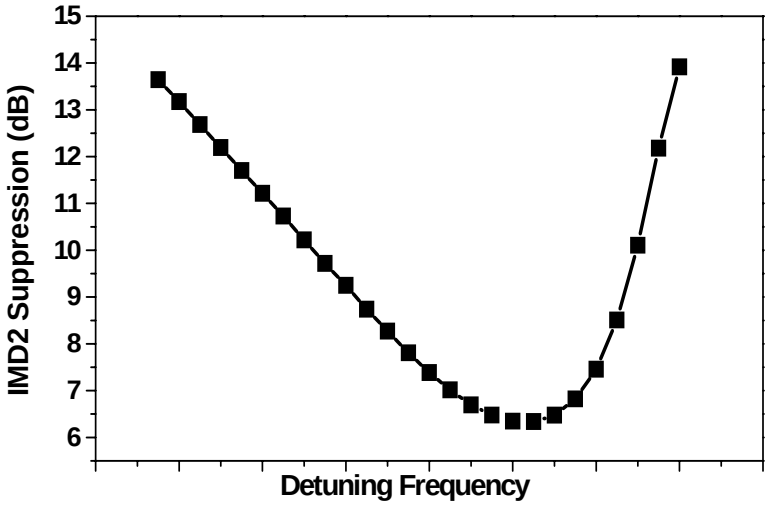

(a)

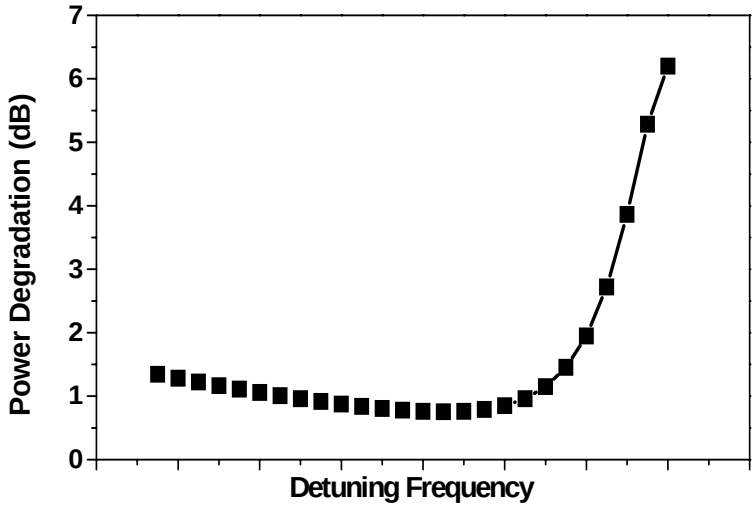

(b)

Figure 3.10 Simulation results. (a) IMD2 suppression according to the detuning frequency (b) Modulation signal power changes. Injection ratio is –8 dB and detuning frequency is within the stable locking range.

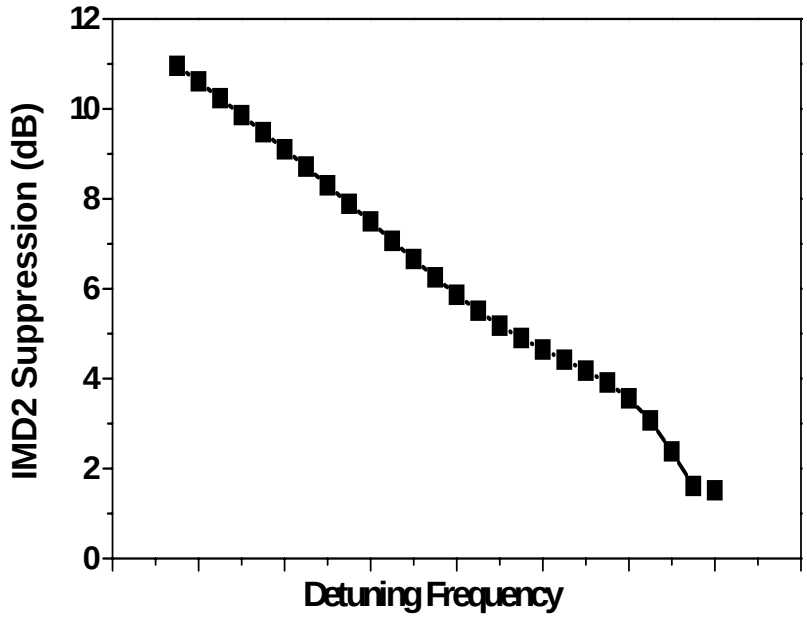

Figure 3.11 Simulation result of IMD2 suppression after the modulation signal power is compensated to the free-running signal power.

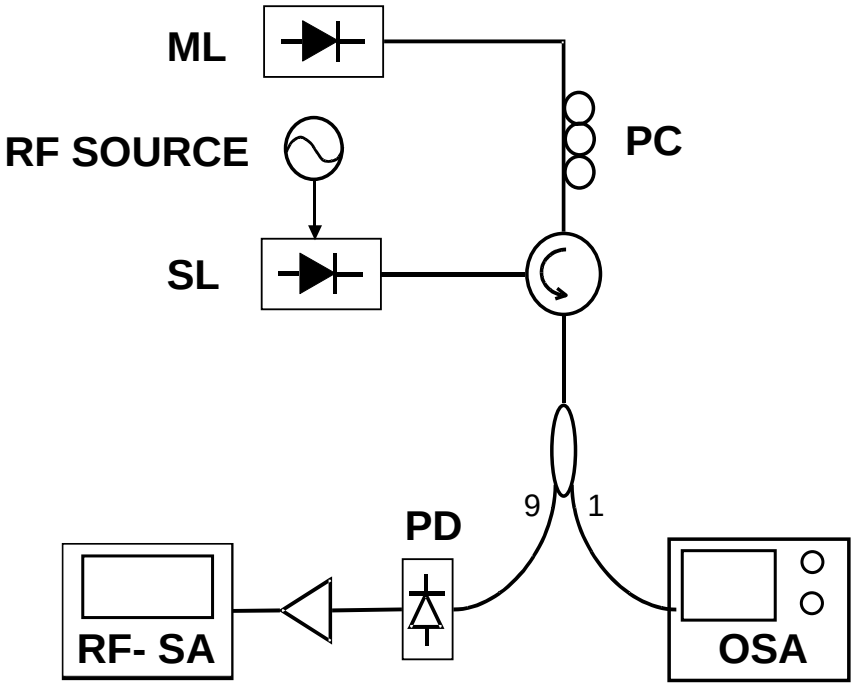

Figure 3.12 Experimental setup. PC: Polarization controller, PD: Photo-Detector, RF-SA: RF Spectrum Analyzer, OSA: Optical Spectrum Analyzer.

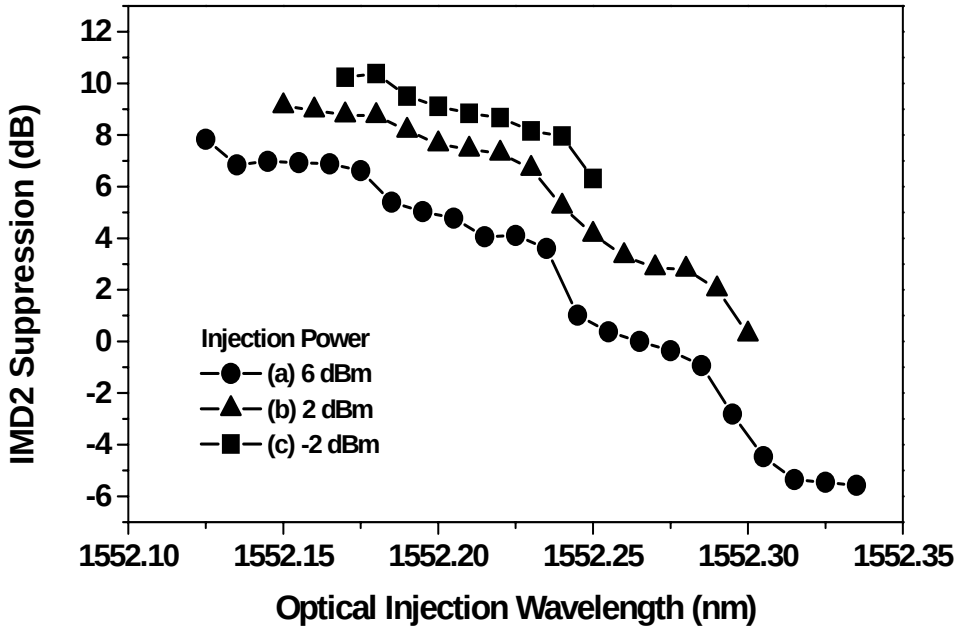

Figure 3.13 IMD2 Suppression within the stable locking range. (a) Optical injection power = 6 dBm, (b) Optical injection power = 2 dBm (c) Optical injection power = -2 dBm.

IV. Nonlinear Distortion Suppression by Sidemode Optical Injection Locking

In section III, as a method of distortion suppression method in directly modulated semiconductor lasers, the optical injection locking technique is investigated. In analog fiber-optic transmission systems, optical injection locking is very attractive method for the various merits such as distortion suppression, laser chirp reduction, and noise suppression. However, optical injection locking occurs within the relatively narrow lasing frequency detuning range between the ML and SL. This may limit the applicability of the injection locking technique.

To solve this problem, sidemode optical injection locking is considered. In this scheme, light is injected into a highly suppressed DFB laser Fabry-Perot mode instead of the DFB laser main-mode. This technique has been proposed as a solution of waveform reshaping and noise suppression in wavelength conversion technique [23, 24]. In sidemode optical injection locking, as the sidemode power is very low, the unstable locking characteristics due to mode beating between the ML and SL do not easily occur and the stable locking range can be extended. In this section, the validity of sidemode optical injection locking is investigated by observing the laser nonlinear distortion suppression such as harmonic distortion and intermodulation distortion. Moreover, the stable locking range extension will be shown compared with main-mode injection locking.

A. Sidemode Injection Locking Characteristics

Fig. 3-10 shows the experimental setup used for our investigation. The experimental setup is equal to the section III-C experiment because our purpose is to measure the nonlinear distortion suppression and stable locking range. Other experiment condition and optical elements are all equal to the previous experiment.

Fig. 4-1 shows the optical spectra before optical injection and after optical injection. Fig 4-1(a) shows the SL optical spectrum in free-running (no optical injection). When a sufficient amount of the ML light is injected into the sidemode marked as -1 mode, the main-mode is significantly suppressed and the sidemode becomes dominant as can be seen in Fig. 4-1(b). The stable locking range can be estimated by the range of main-mode suppression as was done for a Fabry-Perot laser in the reference [25]. However, because a DFB laser is used, high injection power is needed to lock the sidemode and to suppress the main-mode sufficiently. For the sidemode to become a dominant mode, the sidemode threshold gain should be lower than the main-mode and this can be achieved by high external light injection. Therefore, the necessary injection power and main-mode suppression range is changed according to the selected sidemodes. By using the sidemodes near the main-mode, the SL locks to the ML easily and has a wide locking range with relatively low injection power.

In order to investigate the sidemode optical injection phenomena in detail, the dependence of the SL main-mode power changes on the ML injection wavelength and the optical power is observed. The ML wavelength is selected

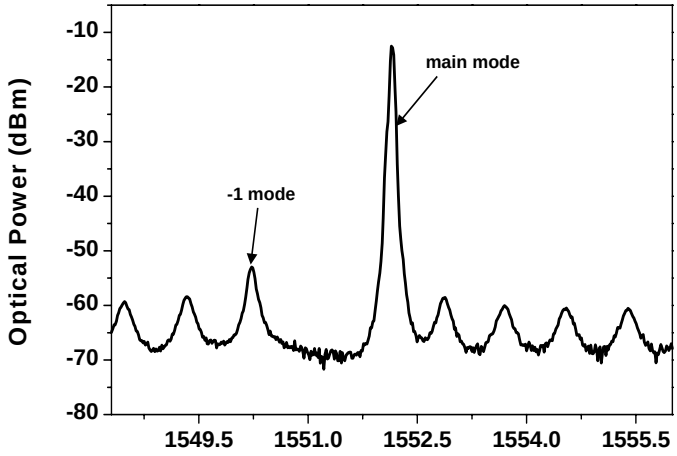

(a)

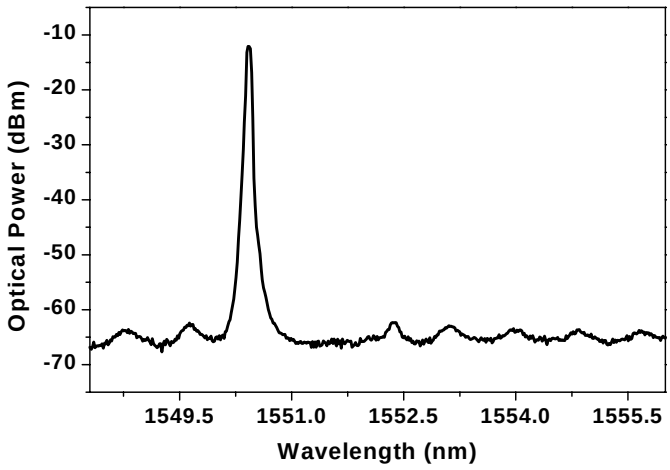

(b)

Figure 4.1 Optical spectra of the SL. (a) Free-running (no optical injection) (b) Injection locking at the target mode (-1 mode).

around the target mode located at 1550.2 nm (-1 mode) and is changed from 1549.8 nm to 1550.8 nm in steps of 0.01nm. The ML optical power is selected at –2 dBm, 2 dBm, and 6 dBm, which is measured at the circulator output toward the SL. The SL bias current is maintained at 18 mA, which corresponds to 2.5 times the level of the threshold. Fig. 4-2 shows the main-mode power that is normalized by the free-running main-mode peak power. As shown in the figure, with larger ML optical power, the main-mode is further suppressed and the main-mode suppression range widens. This means that with a larger ML optical power, the locking range can widen. The usual asymmetric locking range characteristics are also observed. For 6 dBm optical injection power, the main-mode can be suppressed more than 40 dB, and the stable locking range is estimated at about 58 GHz. Under similar injection conditions, the stable locking range for the main DFB mode is measured to be about 26 GHz. Therefore, by means of sidemode optical injection, the stable locking range can be double. The reason for this wide stable locking range is believed that, since the sidemode power is very low, unstable locking characteristics due to mode beating between the ML and SL do not affect the locking range. In addition, similar to the mode dependence of the stable locking range in Fabry-Perot lasers, the locking range is the case of DFB laser sidemode injection is related to the injection mode and can be wider than the main-mode injection locking range [26, 27].

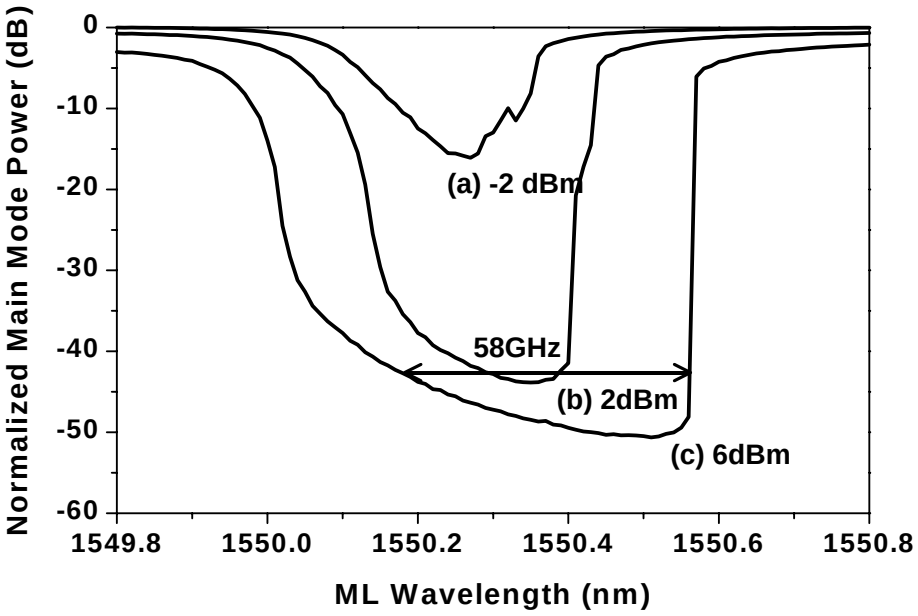

Figure 4.2 Normalized main-mode power according to the ML injection wavelength. (a) ML power is –2 dBm (b) ML power is 2 dBm. (c) ML power is 6 dBm.

B. Nonlinear Distortion Suppression by Sidemode Optical Injection Locking

Next, the nonlinear distortion characteristics of directly modulated lasers are investigated in case of sidemode optical injection locking. For generating subcarriers, the SL is directly modulated by two RF signals (f_1 = 2.8 GHz and f_2 = 2.9 GHz). In this experiment, we measure the power of the second harmonic distortion (SHD), second order intermodulation distortion (IMD2), and third order intermodulation distortion (IMD3). The SHD is defined as the ratio of power at frequency $2f_2$ to the power at fundamental frequency. The IMD2 and IMD3 are defined as the ratio of power at frequency f_1+f_2 and at frequency $2f_2-f_1$, respectively, to the power at fundamental frequency. For the sidemode optical injection experiment, the injection light power is 6 dBm and the wavelength is set at 1550.434 nm. Under these conditions, the laser main-mode is suppressed about 50 dB. Fig. 4-3 shows the detected RF power of the second harmonic and the second order intermodulation product. The input RF power is measured at the RF signal generator output. The linearly fitted lines show the slope of fundamental frequency power is one and those of the second harmonic power and IMP2 are two. These are the usual characteristics of modulation frequency power, second harmonic power and IMP2. As can be seen in the figure, the SHD and IMD2 are suppressed by more than 10 dB by means of sidemode optical injection locking. Like main-mode injection locking, these are the result of a resonance frequency shift toward higher frequency. In this figure, the fundamental frequency power is slightly decreased after light injection. This is also due to a shift of resonance

frequency.

Then, reduction of IMD3 is observed. Intermodulation distortion occurs when the laser is modulated by two or more subcarriers. For narrow band applications, the IMP3 caused by two closely spaced subcarriers is the most important, because the IMP3 signals fall close to the original subcarrier frequencies. Fig. 4-4 shows the power of third order intermodulation distortion product (IMP3) for the free-running and for sidemode optical injection locking according to the input RF power. The slope of IMP3 is three, as expected. From fig. 4-4, the IMD3 can be suppressed by more than 10 dB, and the spurious-free dynamic range (SFDR) can be estimated by linear-fitting [5]. As a result, 3 dB dynamic range is enhanced for the IMD3. Fig 4-5 is an example of IMD suppression of the injection locked laser. Input RF power is –7 dBm.

C. Comparison between Main-mode Injection Locking and Sidemode Injection Locking

Finally, it is compared the ML detuning range and distortion suppression ability of sidemode and main-mode optical injection locking. For comparison, the IMD2 suppression of both cases is measured. The experimental setup is also equal to the fig. 3-10. The laser bias current is 18 mA, and the injection power is set at 2dBm. The experiment methods also equal to the section III-C experiment.

Fig. 4-6 shows the IMD2 suppression according to the injected light wavelength. Fig. 4-6(a) is the main-mode optical injection case. This result is already shown in fig. 3-11. Using this result, the comparison will be made. For

the given injected light power, the locking range is determined to be from 1552.15 nm to 1552.3 nm, and this is equal to the 18 GHz. Within the locking range, IMD2 suppression is less than 8 dB. Fig. 4-6(b) is the sidemode optical injection case. Using the same optical injection power, more than 40 dB main-mode suppression range is from 1550.16 nm to 1550.45 nm, which corresponds to the 35 GHz, and within this range the SL locks to the ML. Within this range, the IMD2 suppression is from more than 8 dB to a maximum of 22 dB. As shown in section III-C, the IMD suppression is dependent on the optical injection wavelength, and injection power ratio. Therefore, sidemode injection locking also affected by these parameters. However, some interesting phenomena is that fig. 4-6(a) and fig. 4-6(b) are mirror image shape, that is, when sidemode injection locking is used, the IMD2 is suppressed more at higher wavelength optical injection, and when main-mode injection locking is used, the IMD2 is suppressed more at lower wavelength optical injection. That is thought to be the result of the difference of relaxation oscillation frequency increase and damping factor. However, the experiment for measuring the relaxation oscillation frequency and damping factor is needed to fully analyze these phenomena.

Consequently, by using sidemode injection locking, a wider stable locking range and more IMD suppression is possible compared with the main-mode injection locking using same optical injection power.

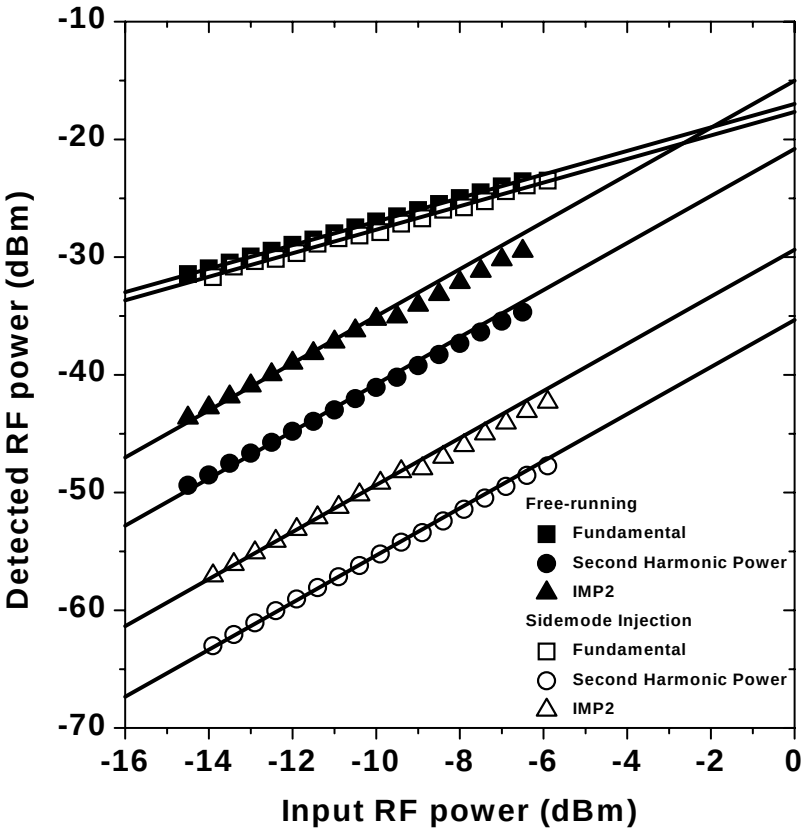

Figure 4.3 Detected RF power according to the input RF power. Second harmonic and second order intermodulation product (IMP2) are shown. The laser is modulated by two RF inputs (2.8 GHz, 2.9 GHz).

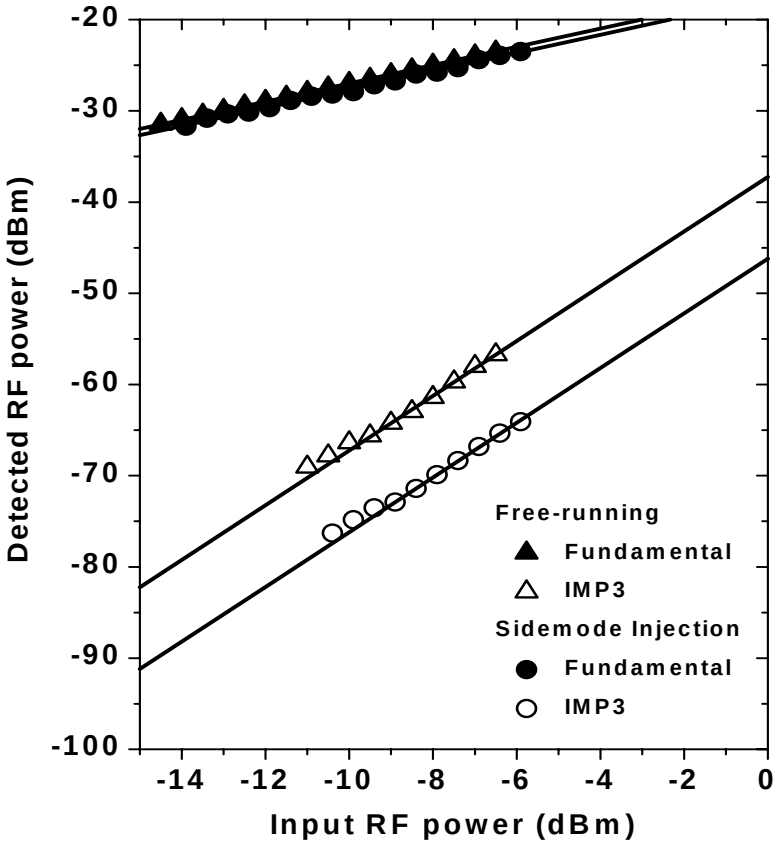

Figure 4.4 Detected RF power according to the input RF power. Third order intermodulation distortion product (IMP3) power is shown. Modulation frequencies are 2.8 GHz and 2.9 GHz.

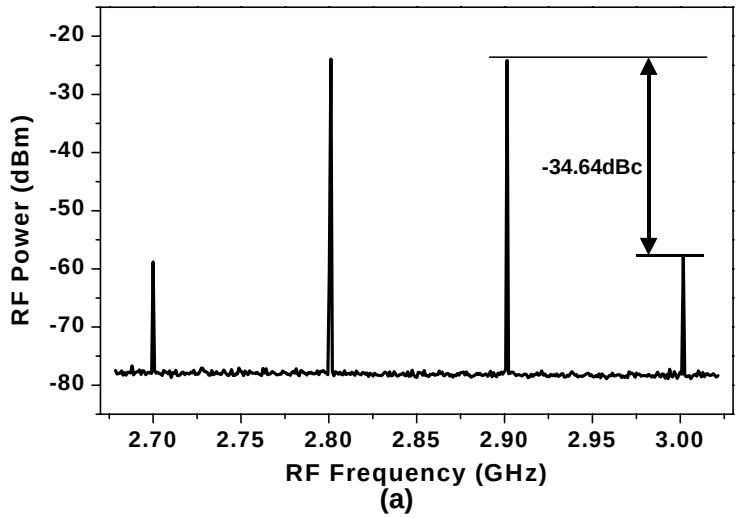

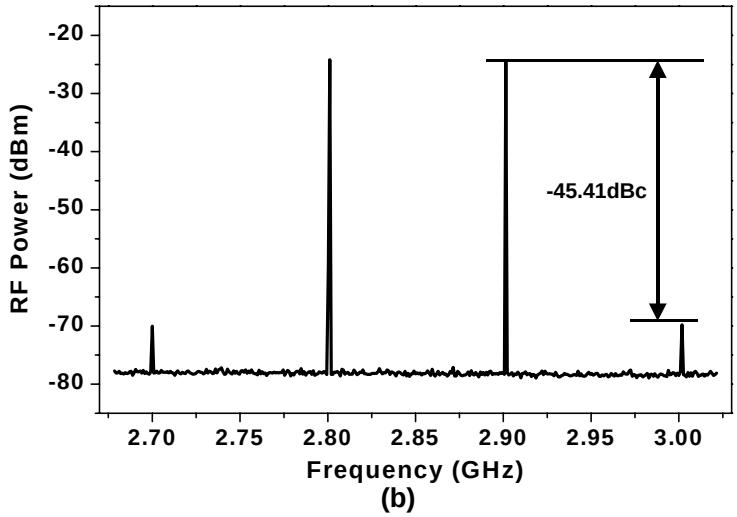

Figure 4.5 RF spectra of two-tone modulation experiment (2.8 GHz and 2.9 GHz). (a) Free-runing state, IMD3 = -34.65 dBc. (b) Injection locked state, IMD3 = -45.41 dBc. Input RF power is –7 dBm.

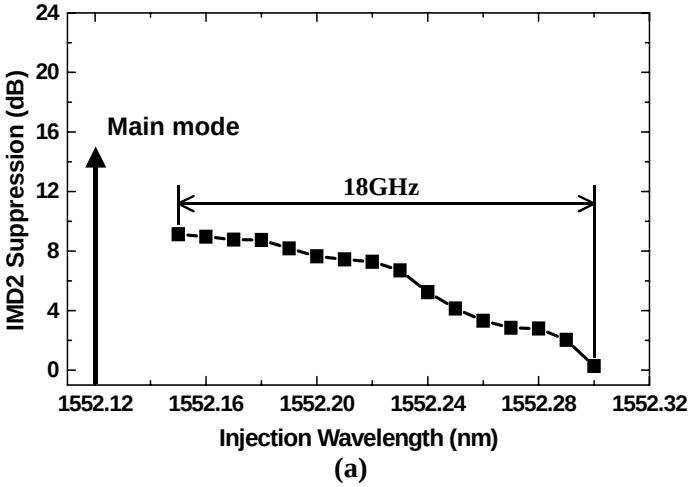

Figure 4.6 IMD2 suppression according to the ML injection wavelength. (a) Main-mode injection locking (b) sidemode injection locking. Injection power is set at 2 dBm.

V. Summary

In analog fiber-optic link, the direct laser modulation method is very simple and cost-effect. However, the direct laser modulation causes nonlinear distortion, which degrade system performance. In the thesis, the laser nonlinear distortion is analyzed and a new distortion suppression method is proposed.

First, the laser nonlinear distortion is investigated by using Volterra series expansion of the laser rate equations. Based on this analytic distortion model, the usual distortion characteristics are observed. Then, as one previously reported distortion suppression method, optical injection locking is introduced. This technique has many advantages such as low chirp, narrow linewidth, and noise reduction besides the distortion suppression by relaxation oscillation frequency increase. To find the characteristics of optical injection locking, the system matrix from the rate equation that contains external light injection is used. From the computer simulation, the validity of nonlinear distortion suppression by optical injection locking is proved. Moreover, the stable locking range dependence on laser parameters is observed. It is found that the large gain suppression factor and bias current can extend the stable locking range, and the large linewidth enhancement factor and differential gain can shrink the stable locking range. The distortion suppression for optical injection wavelength and power is also analyzed by the injection locked laser frequency response simulation and IMD2 suppression experiment. The results show that when the detuning frequency is small, the relaxation oscillation frequency increase is dominant and when large, the damping is grown. When optical

injection power is high, injection locking affects the relaxation oscillation frequency increase and high damping factor. Finally, for extending the stable locking range, sidemode injection locking is proposed. Experimentally, more than 10 dB second harmonic, IMD2, and IMD3 are reduced. Compared with the main-mode injection locking, more distortion suppression and a wider stable locking range are achieved.

This thesis mainly focused on the nonlinear distortion and its suppression by injection locking. For investigating, the laser rate equation model is used, and distortion suppression experiments are performed. However, the frequency response experiment is needed for further precise analysis, and this remains for future work.

VI. References

[1] W, I, Way, “Broadband Hybrid Fiber/Coax Access System Technologies,” Academic Press, 1999

[2] R. Olshansky, “Subcarrier multiplexing lightwave systems for broadband distribution.” *J. Lightwave Technol.*, vol. 7, no. 9, pp. 1329-1342, September 1989.

[3] G. Morthier, F. Libbrecht, K. David, P. Vankwikelberge, and R. G. Baets, “Theoretical investigation of the second-order harmonic distortion in the AM response of 1.55 μm F-P and DFB lasers.” *IEEE J. Quantum Electron.*, vol. 27, no. 8, pp. 1990-2002, August 1991.

[4] L. Zhang and D. A. Ackerman, “Second- and third-order harmonic distortion in DFB lasers,” *IEEE J. Quantum Electron.*, vol. 31, no. 11, pp. 1974-1980, November 1995.

[5] X. G. Meng, T. Chau, and C. Wu, “Improved intrinsic dynamic distortions in directly modulated semiconductor lasers by optical injection locking,” *IEEE Trans. Microwave Theory and Tech.*, vol. 47, no. 7, pp. 1172-1176, July 1999.

[6] A. V. D. Grijp, J. C. Koopman, L. J. Meuleman, A. J. A. Nicia, E. Roze, and J. H. C. Heuven, “Novel electro-optic feedback technique for noise and distortion reduction in high-quality analogue optical transmission video signal,” *Electron. Lett*., vol. 17, no. 11, pp. 361-362, 1981.

[7] L. S. Fock and R. S. Tucker, “Simultaneous reduction of intensity noise and distortion in semiconductor lasers by feedforward compensation,” *Electron. Lett.,*vol. 27, no. 14, pp. 1297-1298, 1991.

[8] H. M. Salgado, J. J. O’Reilly, “Experimental validation of Volterra series nonlinear modeling for microwave subcarrier optical systems,” *IEE Proc. – Optoelectron.*, vol. 143, no. 4, pp. 209-213, August 1996.

[9] W. I. Way, “Large signal nonlinear distortion prediction for a single-mode laser diode under microwave modulation,” *J. Lightwave Technol.,* vol. LT-5, no. 3, pp. 305-315, March 1987.

[10] J. Helms, “Intermodulation distortions of broad-band modulated laser diodes,” *J. Lightwave Technol.,* vol. 10, no. 12, December 1992.

[11] J. C. Cartledge, G. S. Burley, “The effect of laser chirping on lightwave system performance,” *J. Lightwave Technol*., vol. 7, no. 3, pp. 568-573, March 1989.

[12] E. D. Bedrosian, and S. O. Rice, “The output properties of volterra system (nonlinear systems with memory) driven by harmonic and gaussian inputs,” *Proc. IEEE*, vol. 59, no. 12, pp. 1688-1707, December 1971.

[13] J. J. Bussgang, L. Ehrman, and J. W. Graham, “Analysis of nonlinear systems with multiple inputs,” *Proc. IEEE*, vol. 62, no. 8, pp. 1088-1119, August 1974.

[14] T. E. Darcie and G. E. Bodeep, “Lightwave subcarrier CATV transmission systems,” *IEEE Trans. Microwave Theory and Tech.,* vol. 38, pp. 524-533, May 1990.

[15] C. Y. Kuo and E. E. Bergmann, “Second-order distortion and electronic compensation in analog links containing fiber amplifiers,” *J. Lightwave Technol.,* vol. 10, pp. 1751-1759, November 1992.

[16] G. Yabre and J. L. Bihan, “Reduction of nonlinear distortion in directly modulated semiconductor lasers by coherent light injection,” *IEEE J. Quantum Electron*., vol. 33, no. 7, pp. 1132- 1140, July, 1997.

[17] J. C. Cartledge, “Theoretical performance of multigigabit-per-second lightwave systems using injection-locked semiconductor lasers,” *J. Lightwave Technol*., vol.8, no. 7, pp. 1017-1022, 1996.

[18] F. Mogensen, H. Olesen, and G. Jacobsen, “Locking conditions and stability properties for a semiconductor laser with external light injection,” *J. Quantum Electron*., vol. 21, no. 7, pp. 784-793, July 1985.

[19] M. Willatzen, A. Uskov, J. Mørk, H. Olsen, B. Tromborg, and A. –P. Jauho, “Nonlinear gain suppression in semiconductor lasers due to carrier heating,” *IEEE Photon. Technol. Lett*., vol. 3, no. 7, pp. 606-609, July, 1991.

[20] G. Wang, R. Nagarajan, D. Tauber, and J. Bower, “Reduction of damping in high-speed semiconductor lasers,” *IEEE Photon. Technol. Lett*., vol. 5, no. 6, pp. 642-645, June, 1993.

[21] S. K. Hwang and J. M. Liu, “Dynamical characteristics of an optically injected semiconductor laser,” *Opt. Commun*., vol. 183, pp. 195-205, September 2000.

[22] M. C. Tatham, I.F. Lealman, C. P. Seltzer, L. D. Westbrook, and D. M. Cooper, “Resonance frequency, damping, and differential gain in 1.5 μm multiple

quantum-well lasers," *J. Quantum Electron*., vol. 28, no. 2, pp. 408-414, February 1992.

[23] K. Inoue and M. Yoshino, "Bistability and waveform reshaping in a DFB-LD with sidemode light injection," *IEEE Photon. Technol. Lett*., vol. 7, no. 2, pp. 164-166, February 1995.

[24] K. Inoue and K. Oda, "Noise suppression in wavelength conversion using a light-injected laser diode," *IEEE Photon. Technol. Lett*., vol. 7, no. 5, pp. 500-501, May 1995.

[25] G. Liu, X. Jin, and S. L. Chuang, "Measurement of linewidth enhancement factor of semiconductor lasers using an injection-locked semiconductor lasers using an injection-locking technique," *IEEE Photon. Technol., Lett*., vol. 13, no. 5, pp. 648-650, May 2001.

[26] J. Luo and M. Osinski, "Multimode small-signal analysis of side-mode injection-locked semiconductor lasers," *Jpn. J. Appl. Phys*., vol. 31, no. 6A, pp. 685-688, June 1992.

[27] Y. Hong and K. A. Shore, "Locking characteristics of a side-mode injected semiconductor laser," *IEEE J. Quantum Electron*., vol. 35, no. 11, pp. 1713-1717, November 1999.

국 문 요 약

직접 변조된 DFB 레이저의 Optical Injection Locking 상태에서의 비선형 왜곡 해석

본 논문에서는 직접 변조된 DFB 레이저의 비선형 왜곡 문제와 이 왜곡 성분을 줄이기 위한 방법인 optical injection locking 의 특성에 대해 살펴 보았다. 또한 optical injection locking 방법의 약점을 보완하기 위한 방법으로 새로운 비선형 왜곡을 줄이는 방법을 제안하였다.

레이저의 이차, 삼차 왜곡 특성은 rate equation 모델을 Volterra series 를 이용하여 해석 하였다. Optical injection locking 의 특성은 주로 rate equation 모델을 수치적으로 해석하여 연구 하였으며, injection locking 에서의 레이저의 안정적인 동작 영역의 레이저 파라미터 의존성을 해석하였다. 또한 optical injection locking 을 이용한 비선형 왜곡 성분 억제에서 외부 광 주입 레이저의 파장과 출력에 따라 비선형 감소량이 다른 특성을 나타내는데, 이를 레이저의 주파수 응답 및 왜곡 성분 감소에 대한 시뮬레이션을 통해 분석하였다. 해석은 perturbation 방법을 이용한 소신호 해석 방법을 이용하였다. 시뮬레이션 결과는 이차 왜곡 성분 감소 실험을 통해 검증하였다.

마지막으로 injection locking 방법의 성능 개선을 위한 방법으로 sidemode injection locking 방법을 제안하였다. Injection locking 방법은 안정적인 동작 영역이 좁다는 약점을 가지고 있다. 외부 광 주입을 DFB 레이저의 주변 모드에 가함으로써 레이저 직접 변조에 따른 왜곡 성분을 크게 줄일 수 있을 뿐만 아니라 주 모드에 외부 광 주입을 하는 경우보다 더

넓은 안정적인 동작 영역을 얻을 수 있다.

핵심 되는 말: 비선형 왜곡, 레이저 직접 변조, optical injection locking, sidemode optical injection locking, 아날로그 광 링크, stable locking range, Volterra series, rate equation